J. Fluid Mech. (1982), *vol.* 120, *pp.* 91–122
Printed in Great Britain

Nonlinear Marangoni convection in bounded layers. Part 1. Circular cylindrical containers

By S. ROSENBLAT, S. H. DAVIS AND G. M. HOMSY
SHD Associates, Inc., 2735 Simpson St, Evanston, IL 60201, U.S.A.

(Received 16 June 1981 and in revised form 14 December 1981)

We consider liquid in a circular cylinder that undergoes nonlinear Marangoni instability. The upper free surface of the liquid is taken to have large-enough surface tension that surface deflections are neglected. The side walls are adiabatic and impenetrable, and for mathematical simplicity the liquid is allowed to slip on the side walls. The linearized stability theory for heating from below gives the critical Marangoni number M_c as a function of cylinder dimensions, surface-cooling condition and Rayleigh number. The steady nonlinear convective states near M_c are calculated using an asymptotic theory, and the stability of these states is examined. At simple eigenvalues M_c the finite-amplitude states are determined. We find th at the Prandtl number of the liquid influences the stability of axisymmetric states, distinguishing upflow at the centre from downflow. Near those aspect ratios corresponding to double eigenvalues M_c, where two convective states of linear theory are equally likely, the nonlinear theory predicts sequences of transitions from one steady convective state to another as the Marangoni number is increased. These transitions are determined and discussed in detail. Time-periodic convection is possible in certain cases.

1. Introduction

Consider a uniform layer of liquid having infinite horizontal extent, bounded on the bottom by a solid plate and having a free surface on the top. When the plate is heated with respect to the gas at the free surface, a purely conductive static state may exist, in which β is the (constant) magnitude of the temperature gradient. If the free surface possesses surface tension σ, the variations $\sigma(T)$ of surface tension with temperature T can induce *Marangoni instability*. This thermocapillary instability was identified and explained by Pearson (1958), who showed, using a linear stability theory, that a critical value of the Marangoni number M must be exceeded before the conductive state becomes unstable. Here

$$M = \frac{|d\sigma/dT|_0 \beta d^2}{\kappa_0 \mu_0}, \tag{1.1}$$

where $d\sigma/dT$ is the (negative) rate of change of surface tension with temperature, the subscript zero denoting a constant value at a given reference temperature T_0; d is the thickness of the undisturbed layer, and κ_0 and μ_0 are respectively the thermal diffusivity and dynamic viscosity of the liquid.

The critical value M_c of M depends on other parameters: the surface Biot number L, which is the non-dimensional version of the heat-transfer coefficient at the free surface,

and a capillary number C, which is a non-dimensional version of the mean surface tension $\sigma_0 \equiv \sigma(T_0)$. Here

$$C = \mu_0 \kappa_0 / \sigma_0 d. \tag{1.2}$$

Pearson (1958) limited his analysis to $C \to 0$, which means that the free surface does not deform as a result of disturbances. He finds, for $L = 0$ and a perfectly conducting lower boundary, $M_c \simeq 79{\cdot}6$ in the absence of gravity.

When a vertical gravity field is present, so that the layer is heated from below, Nield (1964) showed, using Pearson's model, that buoyancy-induced instabilities and thermocapillary instabilities reinforce one another.

Since the work of Pearson and Nield, linear stability theory on the Marangoni convection problem has been extended in several directions to include two dynamical phases, $C \neq 0$, and further effects of an imposed vertical gravity field (Scriven & Sternling 1964; Smith 1966; Zeren & Reynolds 1972). A recent survey (Sørensen 1979) discusses these as well as many other extensions. Palmer & Berg (1971) find that the theory of Nield (1964) predicts well the experimental conditions for the onset of convection in shallow layers.

As in the case of Rayleigh–Bénard convection due to buoyancy effects, the horizontal planform of the convective state and the amplitude of the motion (and heat transfer) are undetermined by linear stability theory. In addition as in Rayleigh–Bénard convection, the critical point M_c, corresponding to the critical horizontal wavenumber, is infinitely degenerate; there are an infinite number of planforms allowable by linear theory. Nonlinear effects presumably select from this set those that appear in experiments. The first nonlinear analysis of Marangoni instability is due to Scanlon & Segel (1967). They consider an infinite-Prandtl-number fluid, an infinitely deep layer, and only *two* planform functions from the infinite set. Their prediction is that hexagonal-cells is the only planform that exists and is stable when the conductive state becomes unstable. Hexagons exist and are stable for an interval of $M < M_c$ so that subcritical convection is predicted. They do not attempt to enlarge the set of planform functions beyond the chosen two. However, their prediction is in qualitative accord with experimental observations. Koschmieder (1967) always found very regular hexagons in shallow layers, the regularity stemming from the precise thermal controls used. These pictures should be compared with those of Bénard (1900) who found irregular, polygonal cells in convection dominated by thermocapillarity.

The only other nonlinear analysis of Marangoni instability is due to Kraska & Sani (1979). They considered *six* planform functions (including those of Scanlon & Segel), and also completed a nonlinear analysis. However, they encountered difficulties in analysing the stability of their nonlinear states and found a lack of closure in adding *any seventh* state to the original six. These difficulties may be related to the adjoint operator they defined, which seems not to be appropriate to the problem.

In the present studies we address the problem of Marangoni instabilities in a cylinder of finite size. Our interest is to explore the nonlinear interactions near $M = M_c$, and, in particular, transitions from one convective state to another that may occur at supercritical conditions. Given the difficulty of such a study, we make several simplifying assumptions. (i) We let the capillary number $C \to 0$. Hence, the top free surface is non-deformable. In addition, we take the contact angle at the side walls to be compatible with a flat free surface. Thus, in the basic, conductive state there are no

menisci, and in the convective state the free surface remains flat. (ii) In order to allow the linear stability theory to be solved using normal modes (separation of variables), we idealize the side-wall boundary conditions in the following way. The side wall consists of a circular cylinder through which there is zero heat flux and zero mass flow. However, we allow the wall to be 'slippery' so that the no-slip condition is replaced by the condition of zero tangential vorticity. Clearly, such an idealization modifies the predictions of a theory. We discuss in detail some implications of this idealization and suggest how results of such a theory should be applied.

Given the model described, we find the nonlinear convective states and determine their stability. Clearly the presence of the side wall makes the spectrum at $M = M_c$ discrete so that the complete behaviour can be examined. Of course, hexagonal cells for small containers will never appear, since the allowable cell shapes are dominated by the side-wall constraints. We obtain its behaviour and its amplitude, and hence can find all transport quantities of the convection. At certain aspect ratios two linearized modes are equally likely at critical conditions. We analyse such double eigenvalues and find certain strong behaviours. The transitions as M is increased for aspect ratios on one side of the double eigenvalues differ substantially from those on the other side of the double eigenvalue. Such a demarcation of behaviours is characteristic of the nonlinearities, and hence should be observable in experiment.

The technique of nonlinear stability theory we use is due to Rosenblat (1979), who makes an eigenfunction expansion of the nonlinear problem. This 'infinite-matrix' form is systematically simplified by defining a *new small parameter* related to the separation of the eigenvalues (the critical M_c) of the matrix. The results coincide with the usual weakly nonlinear bifurcation theory very near the first M_c, but gives a wider range of validity. It is the wider range that allows us to examine the successive transitions.

2. Formulation

Consider a viscous liquid which partially fills a cylindrical container of circular cross-section. The mean depth of the liquid is d, and the radius of the cylinder is taken to be $a^* = ad$, so that the aspect ratio (ratio of radius to mean depth) is a. The axis of the cylinder is antiparallel to the direction of gravity, and the upper surface of the liquid is open to an ambient gas.

The liquid is assumed to be Newtonian, to have constant viscosity μ_0 and to be heat conducting with constant thermal diffusivity κ_0 and conductivity k_0. The liquid–gas interface has a surface tension σ^*, which varies with temperature according to the formula

$$\sigma^* = \sigma_0 - \sigma_1(T_s^* - T_0), \tag{2.1}$$

where σ_0, σ_1 are constants, T_s^* is the temperature at the interface, and T_0 a reference temperature. The Boussinesq approximation is assumed; the governing equations in the bulk of the liquid are the Navier–Stokes, continuity and energy-balance equations.

We shall work in a cylindrical polar co-ordinate system with the origin at the centre of the bottom boundary. The mean depth of the liquid is at $z^* = d$. The lower boundary is assumed to be a rigid perfectly conducting plane. Surface tension acts at the upper boundary, where the usual stress balance applies. The liquid is assumed to be cooled

at the upper boundary by heat transfer to the gas, characterized by a heat-transfer coefficient h.

The lateral boundary is assumed to be adiabatic. If it were rigid, we would have the no-slip condition. However, we take the idealized, mathematically simpler condition that the side wall is a non-deformable surface on which the tangential vorticity vanishes. To complete the specification of the boundary conditions, we require a condition on the behaviour of the free surface where it meets the edge of the container. In this paper, we shall assume that the 'contact angle' is fixed and is $\frac{1}{2}\pi$.

Under these assumptions, there exists a solution to the basic equations which is the motionless state of heat conduction:

$$\mathbf{v}^* \equiv \mathbf{0}, \tag{2.2a}$$

$$T^* = T_0 + \beta(d - z^*), \tag{2.2b}$$

$$\rho^* = \rho_0[1 - \alpha\beta(d - z^*)], \tag{2.2c}$$

$$\sigma^* = \sigma_0, \quad \eta^* = 0, \tag{2.2d, e}$$

$$\boldsymbol{\tau}^* = \rho_0 g\{(z^* - d) + \tfrac{1}{2}\alpha\beta(z - d)^2\}\mathbf{I}. \tag{2.2f}$$

In (2.2), the asterisks denote dimensional quantities; here η^* and $\boldsymbol{\tau}^*$ are respectively the surface deflection above $z^* = d$ and the stress in the liquid.

We now perturb the *basic state* (2.2), and at the same time introduce appropriate dimensionless forms of the equations and boundary conditions. We scale lengths on the depth d, and write

$$r = r^*/d, \quad z = z^*/d, \quad \eta = \eta^*/d, \tag{2.3}$$

with $\mathbf{r} = (r, \phi, z)$ in cylindrical polar co-ordinates. Unit vectors in the corresponding directions will be denoted $(\hat{\mathbf{r}}, \hat{\boldsymbol{\phi}}, \hat{\mathbf{z}})$. The velocity components are (u, v, w). The liquid occupies the region $0 < r < a$, $0 < z < 1 + \eta$ in this dimensionless co-ordinate system; the equation of the free surface S is

$$z = 1 + \eta(\mathbf{r}_1, t), \tag{2.4}$$

where $\mathbf{r}_1$ is the dimensionless position vector in the horizontal plane, and t is dimensionless time, defined below; the lateral boundary S_L is $r = a$, $0 < z < 1 + \eta$.

Since our interest is focused on motions driven by surface-tension gradients, it is appropriate to base velocities on the Marangoni velocity scale V_M, defined by

$$V_M = \sigma_1 \beta d/\mu_0. \tag{2.5}$$

The time scale will then be d/V_M, so that we write

$$t = t^* V_M/d. \tag{2.6}$$

The equations in the bulk of the liquid for the perturbation field quantities are found to be

$$Pr^{-1} M\left\{\frac{\partial \mathbf{v}}{\partial t} + (\mathbf{v}.\nabla)\,\mathbf{v}\right\} = \nabla.\boldsymbol{\tau} + M^{-1} R\theta\hat{\mathbf{z}}, \tag{2.7}$$

$$\boldsymbol{\tau} = -p\mathbf{I} + [\nabla\mathbf{v} + \nabla\mathbf{v}^{\mathrm{T}}], \tag{2.8}$$

$$\nabla.\mathbf{v} = 0, \tag{2.9}$$

$$M\left\{\frac{\partial \theta}{\partial t} - w + (\mathbf{v}.\nabla)\,\theta\right\} = \nabla^2\theta. \tag{2.10}$$

The boundary conditions are as follows. On the lower horizontal boundary

$$\theta = 0 \quad (z = 0, \quad 0 < r \leqslant a), \tag{2.11a}$$

$$\mathbf{v} = \mathbf{0} \quad (z = 0, \quad 0 < r \leqslant a). \tag{2.11b}$$

On the upper surface S, the heat-transfer condition reads

$$\mathbf{n}.\nabla\theta = \mathbf{n}.\hat{\mathbf{z}} - 1 - L(\theta - \eta) \quad \text{on} \quad S. \tag{2.12a}$$

The kinematic condition becomes

$$\frac{\partial \eta}{\partial t} + u\frac{\partial \eta}{\partial r} + \frac{v}{r}\frac{\partial \eta}{\partial \phi} - w = 0 \quad \text{on} \quad S. \tag{2.12b}$$

It is convenient to decompose the stress condition into an equation normal to the surface and an equation tangential to the surface. If we write normal and tangential components as

$$(\boldsymbol{\tau}.\mathbf{n})_n \equiv (\boldsymbol{\tau}.\mathbf{n}).\mathbf{n}, \quad (\boldsymbol{\tau}.\mathbf{n})_t \equiv (\boldsymbol{\tau}.\mathbf{n}) - [(\boldsymbol{\tau}.\mathbf{n}).\mathbf{n}]\mathbf{n},$$

we obtain the dynamic surface conditions

$$G(\eta + \tfrac{1}{2}\alpha\delta T\eta^2) + MC(\boldsymbol{\tau}.\mathbf{n})_n - 2H\{1 + MC(\eta - \theta)\} = 0 \quad \text{on } S, \tag{2.12c}$$

$$(\boldsymbol{\tau}.\mathbf{n})_t + \mathbf{n} \times \{\mathbf{n} \times \nabla(\eta - \theta)\} = \mathbf{0} \quad \text{on } S, \tag{2.12d}$$

where H is the dimensionless mean curvature.

On the lateral boundary S_L we have that $\mathbf{n}_L = \hat{\mathbf{r}}$, and the boundary conditions there are

$$\frac{\partial \theta}{\partial r} = 0, \quad u = 0 \quad \text{on } S_L, \tag{2.13a, b}$$

$$\frac{\partial}{\partial r}(rv) = \frac{\partial w}{\partial r} = 0 \quad \text{on } S_L. \tag{2.13c}$$

The contact-angle condition becomes

$$\frac{\partial \eta}{\partial r} = 0 \quad \text{on} \quad r = a. \tag{2.14}$$

Finally, we recall the stipulation that the mean depth of the liquid is d. This is effectively a condition of volume conservation, and can be expressed as

$$\int_0^a \int_0^{2\pi} r\eta(r, \phi, t)\, d\phi\, dr = 0. \tag{2.15}$$

The problem to be studied comprises the system of equations (2.7)–(2.10), together with the conditions (2.11)–(2.15). There are seven parameters appearing in the problem. These are:

Marangoni number	$M = \sigma_1 \beta d^2/\mu_0\kappa_0$,	(2.16a)
Rayleigh number	$R = \rho_0 \alpha\beta g d^4/\mu_0\kappa_0$,	(2.16b)
Prandtl number	$Pr = \mu_0/\rho_0\kappa_0$,	(2.16c)
capillary number	$C = \mu_0\kappa_0/\sigma_0 d$,	(2.16d)
aspect ratio	$a = a^*/d$,	(2.16e)

Biot number $L = hd/k_0$, (2.16*f*)

Bond number $G = \rho_0 g d^2/\sigma_0$. (2.16*g*)

For our purposes, we shall consider the Marangoni number as the principal parameter. We shall determine M_c, the critical value of M at which the conduction solution becomes unstable, as a function of the other parameters, that is

$$M_c = M_c(R, Pr, G, C, L, a). \tag{2.17}$$

We shall then investigate the properties of the convection as M increases above M_c for various values of the other parameters.

3. Zero-capillary-number limit

In this paper we shall confine our analysis to the case where the capillary number C is zero. The capillary number is associated with deflection of the free surface, and under most circumstances is small. The limit $C \to 0$ corresponds to a flat surface (Davis & Homsy 1980), a restriction which enables onset of convection to be analysed relatively simply. In this limit (2.12*c*) reduces to

$$G(\eta + \tfrac{1}{2}\alpha\beta d\eta^2) - 2H = 0, \tag{3.1}$$

where the mean curvature H is given by

$$2H = \nabla_1 \cdot \left\{ \frac{\nabla_1 \eta}{[1 + (\nabla_1 \eta)^2]^{\frac{1}{2}}} \right\} \tag{3.2}$$

(∇_1 is the gradient in the horizontal plane). Equation (3.1) is thus a differential equation for the surface deflection $\eta = \eta(r, \phi, t)$, which is to be solved subject to the conditions (2.14) and (2.15). A solution is clearly

$$\eta \equiv 0, \tag{3.3}$$

representing an undeformed free surface. The fact that there can be no other solution in the class of functions η with $|\eta|$ sufficiently small is easily established with the aid of the implicit-function theorem. We confine our attention to weakly nonlinear interactions that apply when M is close to M_c and when convective motions are of small amplitude. Thus surface deflections caused by motion remain small when $C \ll 1$.

On the basis of this reasoning we infer that the upper free surface remains flat and undeformed. The equation of S is now $z = 1$ ($0 \leqslant r < a$), and the outward unit normal to it is $\mathbf{n} = \hat{\mathbf{z}}$. The lateral boundary S_L is $r = a$ ($0 < z < 1$). The problem to be solved in the limit $C \to 0$ therefore comprises the equations (2.7)–(2.10) in the bulk of the liquid, together with boundary conditions as follows. On the lower boundary the conditions are (2.11), or equivalently,

$$\theta = u = v = w = 0 \quad (z = 0, \quad 0 \leqslant r < a). \tag{3.4}$$

On the upper free surface (2.12*a*) reduces to

$$\frac{\partial \theta}{\partial z} + L\theta = 0 \quad (z = 1, \quad 0 \leqslant r < a), \tag{3.5a}$$

while (2.12*b*) becomes simply

$$w = 0 \quad (z = 1, \quad 0 \leqslant r < a). \tag{3.5b}$$

In view of (3.3) the condition (2.12*c*) is redundant. We simplify (2.12*d*) by noting that

$$(\boldsymbol{\tau}.\mathbf{n})_t = \left[\frac{\partial u}{\partial z}+\frac{\partial w}{\partial r}\right]\hat{\mathbf{r}}+\left[\frac{\partial v}{\partial z}+\frac{1}{r}\frac{\partial}{\partial \phi}(rw)\right]\hat{\boldsymbol{\phi}},$$

and that

$$\mathbf{n}\times(\mathbf{n}\times\nabla\theta) = -\frac{\partial\theta}{\partial r}\hat{\mathbf{r}}-\frac{1}{r}\frac{\partial\theta}{\partial\phi}\hat{\boldsymbol{\phi}}.$$

Hence (2.12*d*) can be decomposed into the two conditions

$$\frac{\partial u}{\partial z}+\frac{\partial\theta}{\partial r} = 0 \quad (z = 1, \quad 0 \leqslant r < a), \tag{3.5c}$$

$$\frac{\partial v}{\partial z}+\frac{1}{r}\frac{\partial\theta}{\partial\phi} = 0 \quad (z = 1, \quad 0 \leqslant r < a). \tag{3.5d}$$

The lateral boundary conditions (2.13) are

$$\frac{\partial\theta}{\partial r} = u = \frac{\partial}{\partial r}(rv) = \frac{\partial w}{\partial r} = 0 \quad (r = a, \quad 0 < z < 1). \tag{3.6}$$

In summary, therefore, we are required to solve the nonlinear field equations (2.7)–(2.10) subject to the boundary conditions (3.4)–(3.6). With $C = 0$ the Bond number G no longer appears (Davis & Homsy 1980), so we have in place of (2.18) the dependence

$$M_c = M_c(R, Pr, L, a) \tag{3.7}$$

for the critical Marangoni number.

4. Linear stability problem

The critical Marangoni number at which the conduction solution loses stability is determined from linearization of the system (2.7)–(2.10) together with the (linear) boundary conditions (3.4)–(3.6). Although this linear problem is not self-adjoint, we assume the validity of the principle of exchange of stabilities, namely that the growth rate of the most dangerous disturbance changes from real and negative to real and positive as M increases through its critical value. Vidal & Acrivos (1966) show for the linear problem on the infinite layer that this is true, and so we apply the same result to our case.

When the principle of exchange of stabilities holds, the governing equations for the linear stability problem at criticality are

$$\nabla^2\mathbf{v}-\nabla p+M^{-1}R\theta\hat{\mathbf{z}} = 0, \tag{4.1}$$

$$\nabla.\mathbf{v} = 0, \tag{4.2}$$

$$\nabla^2\theta+Mw = 0, \tag{4.3}$$

subject to the boundary conditions (3.4)–(3.6). We apply the operator curl curl to (4.1) and then take the z-component of the resultant equation, obtaining

$$\nabla^4 w+M^{-1}R\nabla_1^2\theta = 0, \tag{4.4}$$

where ∇_1^2 is the planform Laplacian. Thus (4.3) and (4.4) constitute a pair of equations

for the unknown functions w and θ. The appropriate boundary conditions are determined by simplifying (3.4)–(3.6); they are found to be

$$\theta = w = \frac{\partial w}{\partial z} = 0 \quad (z = 0, \quad 0 \leqslant r < a), \tag{4.5}$$

$$\frac{\partial \theta}{\partial z} + L\theta = w = \frac{\partial^2 w}{\partial z^2} - \nabla_1^2 \theta = 0 \quad (z = 1, \quad 0 \leqslant r < a), \tag{4.6}$$

$$\frac{\partial \theta}{\partial r} = \frac{\partial w}{\partial r} = 0 \quad (r = a, \quad 0 < z < 1). \tag{4.7}$$

The system (4.3), (4.4) reduces to a pair of ordinary differential equations through separation of variables. It was in order to effect this reduction that we introduced the artificial condition on the vorticity at the lateral boundary. We put

$$\left.\begin{aligned} w(r, \phi, z) &= \cos m\phi \, J_m(\lambda r) \, Y(z), \\ \theta(r, \phi, z) &= \cos m\phi \, J_m(\lambda r) \, X(z), \end{aligned}\right\} \tag{4.8}$$

where $m = 0, 1, 2, \ldots$ is the *azimuthal wavenumber*, J_m is the Bessel function of order m, and $\lambda > 0$ is determined by the equation

$$J'_m(\lambda a) = 0. \tag{4.9}$$

The condition (4.9) ensures that the lateral boundary conditions (4.7) are both satisfied. The functions $Y(z)$, $X(z)$ are solutions to the eigenvalue problem solved by Nield (1964); cf. appendix. The difference between Nield's problem and the one presently under consideration lies in the significance of the parameter λ: for the unbounded layer λ is the wavenumber in the horizontal plane and can assume all real values, whereas for the finite cylinder λ is restricted to the set of values defined by (4.9).

It is convenient to write (4.9) in the form

$$J'_m(s_{mi}) = 0, \quad \lambda_{mi} = s_{mi}/a, \tag{4.10}$$

where s_{mi} denotes the ith positive zero of J'_m. Thus the integer $i = 1, 2, 3, \ldots$ can be regarded as effectively a *radial wavenumber*, and the functional form of (3.7) is

$$M = M(R, L, a, m, i). \tag{4.11}$$

The critical Marangoni number for fixed R, L and a is then defined to be

$$M_c = M_c(R, L, a) = \min_{m,i} M(R, L, a, m, i). \tag{4.12}$$

Figure 1 shows the variation of M_c with aspect ratio a for fixed values $R = 0$, $L = 0$, and for the six wavenumber pairs $m = 0, 1, 2, 3, 4$, $i = 1$ and $m = 1$, $i = 2$. These six were chosen because for moderate aspect ratios, $0 < a < 2{\cdot}5$ approximately, the critical Marangoni number occurs for one or other of them. We see from figure 1 that $m = 1$, $i = 1$ is the critical wavenumber pair for small aspect ratios, $a < 1{\cdot}15$. On the interval $1{\cdot}15 < a < 1{\cdot}65$ (approximately) the critical mode has $m = 2$, $i = 1$, and with further increase in aspect ratio this is replaced by the axisymmetric mode $m = 0, i = 1$ on $1{\cdot}65 < a < 1{\cdot}9$. Next, the mode $m = 3, i = 1$ is critical in $1{\cdot}9 < a < 2{\cdot}3$, while for $2{\cdot}3 < a < 2{\cdot}5$ the modes $m = 4$, $i = 1$ and $m = 1$, $i = 2$ give nearly the same numerical value of the Marangoni number.

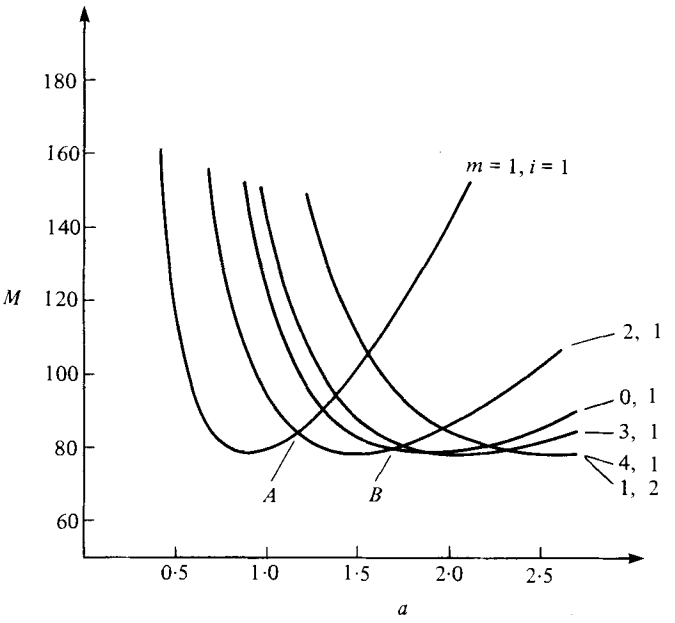

FIGURE 1. Calculated stability curves, M versus a, for $L = 0$, $R = 0$, where m and i are respectively the azimuthal and radial wavenumbers. M_c is the envelope (minima) of the curves.

The ordering of critical modes just described is retained for other values of R and L. In fact, this ordering is a direct consequence of the ordering of the numbers s_{mi} defined by (4.10), which is in turn a consequence of the side-wall boundary conditions; it is not surprising, therefore, that it should be invariant with respect to other physical parameters.

Figure 2 illustrates the variation of critical Marangoni number M_c with aspect ratio a for different values of Rayleigh number R, and at a fixed value $L = 0$. These curves show that M_c decreases as R increases for each value of a. Although not illustrated, computations show that the same behaviour (M_c decreasing with increasing R) occurs when $L \neq 0$.

Figure 3 depicts the variation of M_c with a for various values of surface Biot number L, and at the fixed value $R = 0$. We see that M_c increases with L at each value of a. Computations show the same tendency at non-zero value of Rayleigh number.

The general pattern of behaviour described here is consistent with that obtained by Nield (1964) for an unbounded layer.

5. Eigenfunction expansions

We propose to study the nonlinear stability problem by means of a modified Galerkin procedure. We represent the field quantities by series of functions of the spatial variables, with time-dependent coefficients. Following a suggestion of Eckhaus (1965), we shall take as the basis functions the eigenfunctions of the linear stability problem. The time-dependent coefficients will then be effectively the amplitudes of the appropriate convective modes, determined from nonlinear ordinary differential equations

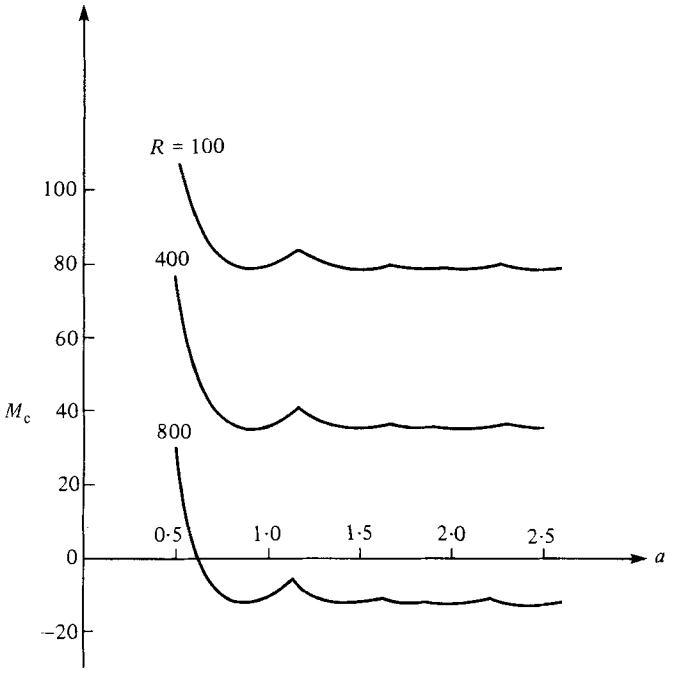

FIGURE 2. Calculated neutral stability curves M_c versus a for $L = 0$ and various values of R. The m-values take the same sequence as in figure 1.

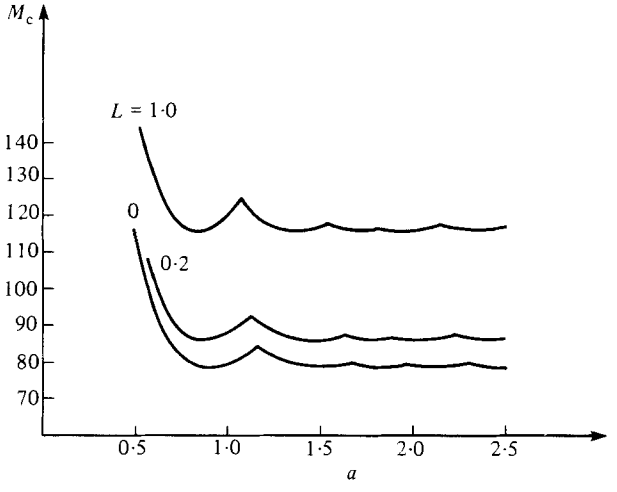

FIGURE 3. Calculated neutral stability curves M_c versus a for $R = 0$ and various values of L. The m-values take the same sequence as in figure 1.

to which the governing partial differential equations reduce. The series are truncated in a *rational* way, according to criteria discussed by Rosenblat (1979).

Galerkin methods require that the function basis of the expansion should constitute a complete set in an appropriate sense. In this regard it has been pointed out by Rosenblat, Homsy & Davis (1981) that the Marangoni number cannot be used as the eigenvalue parameter on which to construct a complete set of eigenfunctions of the

linear stability problem. This is because the expression (4.11) gives M as a single-valued function of R, other parameters being held fixed, and corresponding to this there will be only a single eigenfunction. On the other hand, if (4.11) is solved for R, the resulting expression has the form

$$R = R(M, L, a, m, i), \tag{5.1}$$

and is not single-valued; in fact there is a countably infinite number of solutions of the form (5.1) to the equation (4.11). In other words, there are infinitely many values of R for each value of M, and correspondingly infinitely many eigenfunctions.

Although the critical Marangoni number is given correctly by the results of § 4, the implication of the foregoing paragraph is that the Rayleigh number is the 'true' eigenvalue parameter of the linear stability problem. We need to take this into account in setting up the Galerkin procedure, even though much of the subsequent analysis will become redundant through truncation and approximation.

Let $\hat{M}$ be a fixed value of the Marangoni number, and consider the linear eigenvalue problem

$$V^2\mathbf{v} - \nabla p + \hat{M}^{-1}R\theta\hat{\mathbf{z}} = \mathbf{0}, \tag{5.2}$$

$$\nabla . \mathbf{v} = 0, \tag{5.3}$$

$$\nabla^2\theta + \hat{M}w = 0, \tag{5.4}$$

with boundary conditions (3.4)–(3.6), and with the Rayleigh number R regarded as the eigenvalue parameter. Non-trivial solutions of this boundary-value problem exist for certain values of R, denoted R_{mij}, where m is the azimuthal wavenumber, i is the radial wavenumber, and $j = 1, 2, 3, \ldots$ is the particular value implied by (5.1). Thus

$$R_{mij} = R_j(\hat{M}, L, a, m, i), \tag{5.5}$$

and we assume the ordering $R_{mi1} < R_{mi2} < \ldots$ for other parameters fixed. Graphs of the functions (5.5) can be found in the paper by Rosenblat *et al.* (1981). The integer j is in effect a *vertical wavenumber*.

Corresponding to each eigenvalue R_{mij} there is an eigenvector $(\mathbf{v}_{mij}, \theta_{mij})$ of the linear boundary-value problem. The forms of w_{mij} and θ_{mij} are given by (4.8), while the other two velocity components can be calculated from (5.2) and (5.3). The components, which are required in the subsequent computations, are found to be

$$\left.\begin{aligned} u_{mij} &= (1/\lambda_{mi})\cos m\phi\, J'_m(\lambda_{mi}r)\, DY_{mij}(z), \\ v_{mij} &= (-m/\lambda^2_{mi}r)\sin m\phi\, J_m(\lambda_{mi}r)\, DY_{mij}(z), \\ w_{mij} &= \cos m\phi\, J_m(\lambda_{mi}r)\, Y_{mij}(z), \\ \theta_{mij} &= \cos m\phi\, J_m(\lambda_{mi}r)\, X_{mij}(z), \end{aligned}\right\} \tag{5.6}$$

where X_{mij}, Y_{mij} are the eigensolutions of the eigenvalue problem of Nield with $R = R_{mij}$, $M = \hat{M}$ and $\lambda = \lambda_{mi}$.

In the modified Galerkin–Eckhaus method to be used below we require also the *adjoint* eigenfunctions. The system adjoint to (5.2)–(5.4) is easily shown to be

$$\nabla^2\mathbf{v}^* - \nabla p^* + \hat{M}\theta^*\hat{\mathbf{z}} = \mathbf{0}, \tag{5.7}$$

$$\nabla . \mathbf{v}^* = 0, \tag{5.8}$$

$$\nabla^2\theta^* + \hat{M}^{-1}Rw^* = 0, \tag{5.9}$$

with the adjoint boundary conditions

$$\theta^* = u^* = v^* = w^* = 0 \quad (z = 0, \quad 0 \leqslant r < a), \tag{5.10}$$

$$\frac{\partial \theta^*}{\partial z} + L\theta^* + \frac{\partial w^*}{\partial z} = w^* = \frac{\partial u^*}{\partial z} = \frac{\partial v^*}{\partial z} = 0 \quad (z = 1, \quad 0 \leqslant r < a), \tag{5.11}$$

$$u^* = \frac{\partial}{\partial r}(rv^*) = \frac{\partial w^*}{\partial r} = \frac{\partial \theta^*}{\partial r} = 0 \quad (r = a, \quad 0 < z < 1). \tag{5.12}$$

These forms are consistent with those of Davis (1969) and Davis & Homsy (1980).

The adjoint problem (5.7)–(5.12) is also separable, and the eigenvalues R_{mij} are the same and have the representation (5.5). The adjoint eigenvectors are denoted $(\mathbf{v}^*_{mij}, \theta^*_{mij})$; a relatively simple calculation gives the following explicit representations:

$$\left.\begin{aligned} u^*_{mij} &= \lambda_{mi} \cos m\phi \, J'_m(\lambda_{mi} r) \, DY^*_{mij}(z), \\ v^*_{mij} &= -(m/r) \sin m\phi \, J_m(\lambda_{mi} r) \, DY^*_{mij}(z), \\ w^*_{mij} &= \lambda^2_{mi} \cos m\phi \, J_m(\lambda_{mi} r) \, Y^*_{mij}(z), \\ \theta^*_{mij} &= \cos m\phi \, J_m(\lambda_{mi} r) \, X^*_{mij}(z), \end{aligned}\right\} \tag{5.13}$$

where X^*_{mij}, Y^*_{mij} are solutions of the eigenvalue problem, which is adjoint to that solved by Nield (1964); cf. appendix.

Our purpose is to study the nonlinear evolution of disturbances as the Marangoni number increases through its critical value, and at a *fixed Rayleigh number*. To simplify the discussion we take henceforth $R = 0$, so that pure Marangoni convection will be examined. As a further simplification, and again without essential loss of generality, we take the surface Biot number $L = 0$. The nonlinear system (2.7)–(2.10) can now be written conveniently in the form

$$\nabla^2 \mathbf{v} - \nabla p = M Pr^{-1} \left\{ \frac{\partial \mathbf{v}}{\partial t} + (\mathbf{v} . \nabla) \mathbf{v} \right\}, \tag{5.14}$$

$$\nabla . \mathbf{v} = 0, \tag{5.15}$$

$$\nabla^2 \theta + Mw = M \left\{ \frac{\partial \theta}{\partial t} + (\mathbf{v} . \nabla) \theta \right\}, \tag{5.16}$$

and the boundary conditions are (3.4)–(3.6), with $L = 0$.

We shall solve this problem for values of M close to critical by expanding the field quantities in series of the eigenvectors $(\mathbf{v}_{mij}, \theta_{mij})$ with time-dependent coefficients. First, however, we let $(\mathbf{v}^*_{mij}, \theta^*_{mij})$ denote an eigensolution of the adjoint problem in the case that $\hat{M} = M_c$, the critical value at a fixed aspect ratio for $R = L = 0$. The corresponding eigenvalue is R_{mij}. Because of the ordering of Rayleigh numbers stipulated immediately following (5.5), this means that $R_{mi1} = 0$ for some m and some i. Let $(\mathbf{v}, \theta)$ be a vector with $\nabla . \mathbf{v} = 0$, satisfying the boundary conditions (3.4)–(3.6), and consider the expression

$$Q \equiv \langle \mathbf{v}^*_{mij} . (\nabla^2 \mathbf{v} - \nabla p) + \theta^*_{mij} (\nabla^2 \theta + Mw) \rangle, \tag{5.17}$$

M arbitrary, where $\langle \, \rangle$ denotes integration over the volume $0 \leqslant r < a$, $0 \leqslant \phi < 2\pi$, $0 < z < 1$ occupied by the fluid. Integrating by parts, and noting again that $(\mathbf{v}^*_{mij}, \theta^*_{mij})$ solves the adjoint linear problem with $\hat{M} = M_c$ and $R = R_{mij}$, we easily find that

$$Q = (M - M_c) \langle \theta^*_{mij} w \rangle - M_c^{-1} R_{mij} \langle w^*_{mij} \theta \rangle. \tag{5.18}$$

Observe that $Q = 0$ when $M = M_c$ and $R_{mij} = 0$, which is consistent with the definition of the linear stability problem and its adjoint at criticality.

Next, let $(\mathbf{v}, \theta)$ denote a solution of the nonlinear system (5.14)–(5.16) with boundary conditions (3.4)–(3.6), for some given value of M. Take the scalar product of (5.14) with $\mathbf{v}^*_{mij}$, the product of (5.16) with θ^*_{mij}, add, and integrate over the fluid volume. Using (5.18) we then obtain the equation

$$(M - M_c)\langle\theta^*_{mij} w\rangle - M_c^{-1} R_{mij}\langle w^*_{mij}\theta\rangle = M\left\langle \theta^*_{mij}\frac{\partial\theta}{\partial t} + Pr^{-1}\mathbf{v}^*_{mij}\cdot\frac{\partial\mathbf{v}}{\partial t}\right\rangle + M\langle\theta^*_{mij}(\mathbf{v}\cdot\nabla)\theta + Pr^{-1}\mathbf{v}^*_{mij}\cdot(\mathbf{v}\cdot\nabla)\mathbf{v}\rangle. \quad (5.19)$$

Now choose a finite set $\mathscr{S}$ of eigensolutions $(\mathbf{v}_{mij}, \theta_{mij})$ of the linear stability problem. Let $N \geqslant 1$ be the number of elements in $\mathscr{S}$, and for convenience write

$$\mathscr{S} = \{mij\}, \quad (5.20)$$

which means that an element of the set has azimuthal wavenumber m, radial wavenumber i and vertical wavenumber j. We can thus refer to $mij = p$, say, as the vector wavenumber of an element of $\mathscr{S}$.

We assume that the solution vector $(\mathbf{v}, \theta)$ can be represented, to a good approximation, by a linear combination of elements of the set $\mathscr{S}$, with time-dependent coefficients. Thus we set

$$(\mathbf{v}, \theta) = \sum_{\mathscr{S}} A_{mij}(t)\,(\mathbf{v}_{mij}, \theta_{mij}); \quad (5.21)$$

substitution of (5.21) into (5.19) reduces the latter to a system of N ordinary nonlinear differential equations for the amplitude functions A_{mij}.

The details of this reduction are considerably simplified on account of the following orthogonality relations. First of all we have the bi-orthogonality condition

$$\langle w^*_p \theta_q\rangle = 0 \quad \text{when} \quad p \neq q \quad (5.22)$$

for any two fields with vector wavenumbers p, q. Next, since the azimuthal dependence has a trigonometrical form, we deduce from the orthogonality properties of trigonometrical functions that

$$\langle\theta^*_{mij} w_{nkl}\rangle = \langle\mathbf{v}^*_{mij}\cdot\mathbf{v}_{nkl}\rangle = \langle\theta^*_{mij}\theta_{nkl}\rangle = 0 \quad \text{when} \quad m \neq n, \quad (5.23)$$

for any values of i, j, k, l. Similarly, since the radial dependence has a Bessel-function form, we have

$$\langle\theta^*_{mij} w_{nkl}\rangle = \langle\mathbf{v}^*_{mij}\cdot\mathbf{v}_{nkl}\rangle = \langle\theta^*_{mij}\theta_{nkl}\rangle = 0 \quad \text{when} \quad i \neq k, \quad (5.24)$$

for any values of m, j, n, l.

There remains the question of the choice of the set $\mathscr{S}$. For ease of computation it is desirable that $\mathscr{S}$ should comprise as few elements as reasonably possible. Since we are concerned with the weakly nonlinear interactions that cause the onset of convection, we must certainly include in $\mathscr{S}$ the critical mode (or modes); as pointed out in § 4 the nature of the critical mode depends on the aspect ratio. Finally, $\mathscr{S}$ must include a minimal number of other modes needed to generate nonlinear evolution into convection of the critical mode. By 'minimal' we mean the non-critical modes with the smallest damping rates. As can be seen from (5.19), when M is close to M_c the damping rate of a non-critical mode is determined approximately by the magnitude of R_{mij},

so that we retain only those modes with the smallest values of R_{mij} and neglect all others. A discussion of the procedure and its validity can be found in Rosenblat (1979).

6. Evolution at simple points

We study in this section weakly nonlinear evolution into convection at three specific values of the aspect ratio, namely $a = 0{\cdot}90$, $a = 1{\cdot}50$ and $a = 1{\cdot}80$. As can be seen from figure 1, the loss of stability of the basic conduction state at each of these values is *simple* in the sense that only one mode loses stability as the Marangoni number increases through its critical value. In each case we reduce the problem to a single ordinary nonlinear differential equation of Landau type, and examine its solutions and their stability.

6.1. *The case* $a = 0{\cdot}90$

Figure 1 shows that the critical mode at this aspect ratio is the mode $(m, i, j) = (1, 1, 1)$. We find that

$$M_c = 79{\cdot}5, \tag{6.1}$$

and, by hypothesis, $R_{111} = 0$. Now the quadratic self-interaction of the mode 111 generates the modes $0ij$, $2ij$ with $i, j = 1, 2, \ldots$. Computations show, however, that

$$R_{011} = \min_{i,j} R_{0ij}, \quad R_{211} = \min_{i,j} R_{2ij}, \tag{6.2}$$

and, moreover, that the higher eigenvalues are widely separated from these. For this reason we take the set $\mathscr{S}$ to comprise three modes,

$$\mathscr{S} = \{111, 011, 211\}, \tag{6.3}$$

and substitute into (5.14) the expansion

$$(\mathbf{v}, \theta) = A_{111}(\mathbf{v}_{111}, \theta_{111}) + A_{011}(\mathbf{v}_{011}, \theta_{011}) + A_{211}(\mathbf{v}_{211}, \theta_{211}), \tag{6.4}$$

where the A_{ijk} are functions of time.

Using the orthogonality relations (5.22)–(5.26) to eliminate several of the terms, we obtain the following set of equations:

$$\nu_{111}\dot{A}_{111} = (M - M_c) A_{111} - Z_{111}, \tag{6.5}$$

$$\nu_{011}\dot{A}_{011} = (M - M_c - M_c^{-1} R_{011} f_{011}) A_{011} - Z_{011}, \tag{6.6}$$

$$\nu_{211}\dot{A}_{211} = (M - M_c - M_c^{-1} R_{211} f_{211}) A_{211} - Z_{211}, \tag{6.7}$$

where the dot denotes differentiation with respect to t. Here

$$\nu_{mij} = \frac{M\langle \theta^*_{mij}\theta_{mij} + Pr^{-1}\mathbf{v}^*_{mij}.\mathbf{v}_{mij}\rangle}{\langle \theta^*_{mij} w_{mij}\rangle}, \tag{6.8}$$

$$f_{mij} = \frac{\langle w^*_{mij}\theta_{mij}\rangle}{\langle \theta^*_{mij} w_{mij}\rangle}, \tag{6.9}$$

and the Z_{ijk} are homogeneous quadratic functions of A_{111}, A_{011} and A_{211}. The general form of the Z_{ijk} is given by

$$\langle \theta^*_p w_p\rangle Z_p = M\langle \theta^*_p (\sum_{\mathscr{S}} A_q \mathbf{v}_q.\nabla) \sum_{\mathscr{S}} A_r \theta_r + Pr^{-1}\mathbf{v}^*_p.(\sum_{\mathscr{S}} A_q \mathbf{v}_q.\nabla) \sum_{\mathscr{S}} A_r \mathbf{v}_r\rangle, \tag{6.10}$$

where p, q, r refer to vector wavenumbers.

Each of the two terms on the right of (6.10) contains N^2 integrals when $\mathscr{S}$ has N elements. However, several of these integrals are identically zero by virtue of the orthogonality relations (5.22)–(5.24). In the present case we find that, for the mode 111, only 4 of the 9 integrals are non-zero, and we obtain for the associated quadratic nonlinearity an expression of the form

$$d_{111}Z_{111} = MA_{111}(\alpha_0 A_{011} + \alpha_2 A_{211}), \tag{6.11}$$

where

$$d_{mij} = \langle \theta^*_{mij} w_{mij} \rangle, \tag{6.12}$$

and where

$$\alpha_m = \langle \theta^*_{111}(\mathbf{v}_{111}.\nabla\theta_{m11} + \mathbf{v}_{m11}.\nabla\theta_{111}) + Pr^{-1}\mathbf{v}^*_{111}.(\mathbf{v}_{111}.\nabla\mathbf{v}_{m11} + \mathbf{v}_{m11}.\nabla\mathbf{v}_{111})\rangle, \tag{6.13}$$

for $m = 0$ and 2. Using similar considerations, we obtain

$$d_{011}Z_{011} = M(\alpha_{01}A^2_{111} + \alpha_{00}A^2_{011} + \alpha_{02}A^2_{211}), \tag{6.14}$$

$$d_{211}Z_{211} = M(\alpha_{21}A^2_{111} + \alpha_{202}A_{011}A_{211}), \tag{6.15}$$

where

$$\alpha_{mk} = \langle \theta^*_{m11}\mathbf{v}_{k11}.\nabla\theta_{k11} + Pr^{-1}\mathbf{v}^*_{m11}.(\mathbf{v}_{k11}.\nabla)\mathbf{v}_{k11}\rangle \tag{6.16}$$

for $m = 0$, $k = 0, 1, 2$ and $m = 2$, $k = 1$, and

$$\alpha_{202} = \langle \theta^*_{211}(\mathbf{v}_{011}.\nabla\theta_{211} + \mathbf{v}_{211}.\nabla\theta_{011}) + Pr^{-1}\mathbf{v}^*_{211}.(\mathbf{v}_{011}.\nabla\mathbf{v}_{211} + \mathbf{v}_{211}.\nabla\mathbf{v}_{011})\rangle. \tag{6.17}$$

Equations (6.5)–(6.7) are the evolution equations for the mode 111 at the aspect ratio $a = 0{\cdot}9$. The null solution, $A_{111} = A_{011} = A_{211} = 0$, corresponds to the conduction state, and at fixed Rayleigh number, $R = R_{111} = 0$, is stable for $M < M_c$ and unstable for $M > M_c$.

To study bifurcation from the critical point and the evolution of convection in the neighbourhood of $M = M_c$, we can simplify the system (6.5)–(6.7) in the following way. The modes A_{011} and A_{211} are relatively strongly damped at $M = M_c$, and are present only because of the quadratic self-interaction of the critical mode A_{111}. Hence we can neglect the time-derivative terms in (6.6) and (6.7), and replace M by M_c in these equations. Moreover, when M is close to M_c the magnitudes of A_{011} and A_{211} are small compared with A_{111}; hence in the right-hand sides of (6.14) and (6.15) we can neglect the quadratic terms involving A_{011} and A_{211} by comparison with the terms involving A^2_{111}. Taking these approximations together, and substituting (6.14) and (6.15) into (6.6) and (6.7) respectively, we obtain

$$A_{011} = \frac{-M_c^2\alpha_{01}A^2_{111}}{R_{011}f_{011}d_{011}}, \quad A_{211} = \frac{-M_c^2\alpha_{21}A^2_{111}}{R_{211}f_{211}d_{211}}. \tag{6.18}$$

We now substitute (6.18) into (6.11), and then substitute the latter, with M replaced by M_c, into (6.5). This gives the single equation

$$\nu_{111}\dot{A}_{111} = (M - M_c)A_{111} - \omega_{111}A^3_{111}, \tag{6.19}$$

where

$$\omega_{111} = -\frac{M_c^3}{d_{111}}\left(\frac{\alpha_0\alpha_{01}}{R_{011}f_{011}d_{011}} + \frac{\alpha_2\alpha_{21}}{R_{211}f_{211}d_{211}}\right). \tag{6.20}$$

Equation (6.19) is the Landau equation for the evolution of the critical mode 111. The coefficients ν_{111}, ω_{111} are determined by numerical integration of the appropriate

Pr	$\nu_{111} \times 10^{-4}$	$\omega_{111} \times 10^{-3}$
0·1	0·37	1·2
1·0	0·13	0·16
10·0	0·10	0·11
∞	0·10	0·10

TABLE 1

products of eigenfunctions. The computations have been performed at various values of Prandtl number and some results are shown in table 1. We infer from the calculations that

$$\nu_{111} > 0, \quad \omega_{111} > 0, \tag{6.21}$$

for all Prandtl numbers.

From (6.19) and (6.21) we infer that a solution bifurcates from the critical value M_c having the representation

$$A_{111} = \pm [(M - M_c)/\omega_{111}]^{\frac{1}{2}}. \tag{6.22}$$

The solution exists only for $M > M_c$ (supercritically), and is known from elementary bifurcation theory to be stable. Because of the representation (6.4), we conclude that at aspect ratio $a = 0{\cdot}9$ the onset of convection is supercritical and, for small $M - M_c$, has to leading order the form of a *non*-axisymmetric mode with azimuthal wavenumber 1.

6.2. *The case* $a = 1{\cdot}50$

From figure 1 we see that at this aspect ratio the critical mode is $(m, i, j) = (2, 1, 1)$. The critical Marangoni number is

$$M_c = 79{\cdot}5, \tag{6.23}$$

with $R_{211} = 0$. The quadratic interaction of the mode 211 with itself generates the modes $0ij$, $4ij$, with $i, j = 1, 2, 3, \ldots$, but because of the ordering of the associated eigenvalues we neglect all except the modes 011 and 411. Thus

$$\mathscr{S} = \{211, 011, 411\}. \tag{6.24}$$

Since the index j indicating the vertical mode is always unity, we simplify the notation by dropping the last subscript. Thus

$$(\mathbf{v}, \theta) = A_{21}(\mathbf{v}_{21}, \theta_{21}) + A_{01}(\mathbf{v}_{01}, \theta_{01}) + A_{41}(\mathbf{v}_{41}, \theta_{41}). \tag{6.25}$$

We substitute (6.25) into (5.19) to obtain a system of three ordinary differential equations for the amplitudes, namely

$$\nu_{21} \dot{A}_{21} = (M - M_c) A_{21} - Z_{21}, \tag{6.26}$$

$$\nu_{01} \dot{A}_{01} = (M - M_c - M_c^{-1} R_{01} f_{01}) A_{01} - Z_{01}, \tag{6.27}$$

$$\nu_{41} \dot{A}_{41} = (M - M_c - M_c^{-1} R_{41} f_{41}) A_{41} - Z_{41}, \tag{6.28}$$

where the coefficients have the forms (6.8)–(6.10). Proceeding as in the previous case, we find that

$$d_{21} Z_{21} = M A_{21} (\beta_0 A_{01} + \beta_4 A_{41}), \tag{6.29}$$

where

$$\beta_m = \langle \theta_{21}^* (\mathbf{v}_{21} \cdot \nabla \theta_{m1} + \mathbf{v}_{m1} \cdot \nabla \theta_{21}) + Pr^{-1} \mathbf{v}_{21}^* \cdot (\mathbf{v}_{21} \cdot \nabla \mathbf{v}_{m1} + \mathbf{v}_{m1} \cdot \nabla \mathbf{v}_{21}) \rangle \tag{6.30}$$

Pr	$\nu_{21} \times 10^{-4}$	$\omega_{21} \times 10^{-2}$
0·1	0·37	6·2
1·0	0·13	0·98
10·0	0·10	0·50
∞	0·10	0·45

TABLE 2

for $m = 0$ and 4; also

$$d_{01} Z_{01} = M(\beta_{02} A_{21}^2 + \beta_{00} A_{01}^2 + \beta_{04} A_{41}^2), \tag{6.31}$$

$$d_{41} Z_{41} = M(\beta_{42} A_{21}^2 + \beta_{404} A_{01} A_{41}), \tag{6.32}$$

where

$$\beta_{mk} = \langle \theta_{m1}^* \mathbf{v}_{k1} . \nabla \theta_{k1} + Pr^{-1} \mathbf{v}_{m1}^* . (\mathbf{v}_{k1} . \nabla) \mathbf{v}_{k1} \rangle, \tag{6.33}$$

for $m = 0$, $k = 0, 2, 4$ and $m = 4$, $k = 2$, and

$$\beta_{404} = \langle \theta_{41}^* (\mathbf{v}_{01} . \nabla \theta_{41} + \mathbf{v}_{41} . \nabla \theta_{01}) + Pr^{-1} \mathbf{v}_{41}^* . (\mathbf{v}_{01} . \nabla \mathbf{v}_{41} + \mathbf{v}_{41} . \nabla \mathbf{v}_{01}) \rangle. \tag{6.34}$$

Using the same reasoning as before, we can solve (6.27) and (6.28) approximately to find A_{011} and A_{411} in terms of A_{211}^2. We obtain

$$A_{01} = \frac{-M_c^2 \beta_{02} A_{21}^2}{R_{01} f_{01} d_{01}}, \quad A_{41} = \frac{-M_c^2 \beta_{42} A_{11}^2}{R_{41} f_{41} d_{41}}. \tag{6.35}$$

Substituting (6.35) and (6.29) into (6.26), we find that the latter reduces to the simple Landau equation

$$\nu_{21} \dot{A}_{21} = (M - M_c) A_{21} - \omega_{21} A_{21}^3, \tag{6.36}$$

where

$$\omega_{21} = -\frac{M_c^3}{d_{21}} \left(\frac{\beta_0 \beta_{02}}{R_{01} f_{01} d_{01}} + \frac{\beta_4 \beta_{42}}{R_{41} f_{41} d_{41}} \right). \tag{6.37}$$

Computed values of the coefficients ν_{21}, ω_{21} for various Prandtl numbers are given in table 2, from which it can be seen that both coefficients are always positive. We infer that

$$A_{21} = \pm [(M - M_c)/\omega_{21}]^{\frac{1}{2}} \tag{6.38}$$

represents a stable supercritical conduction solution for $M - M_c$ small, and corresponds to a non-axisymmetric mode with azimuthal wavenumber 2.

6.3. *The case* $a = 1{\cdot}80$

Figure 1 shows that the critical mode at this aspect ratio is the axisymmetric mode $(m, i, j) = (0, 1, 1)$. We find that

$$M_c = 79{\cdot}7, \tag{6.39}$$

with $R_{011} = 0$. The quadratic self-interaction of this mode generates all the modes $0ij$ with $i, j = 1, 2, \ldots$, but by virtue of the ordering of the eigenvalues R_{0ij} we retain only the mode 021. Thus

$$\mathscr{S} = \{011, 021\}, \tag{6.40}$$

and we substitute the expansion (with $j = 1$ assumed)

$$(\mathbf{v}, \theta) = A_{01}(\mathbf{v}_{01}, \theta_{01}) + A_{02}(\mathbf{v}_{02}, \theta_{02}) \tag{6.41}$$

Pr	$\nu_{01} \times 10^{-4}$	$\gamma_0 \times 10^{-2}$	$\omega_{01} \times 10^{-3}$
0·1	0·36	0·32	1·8
1·0	0·12	−0·19	0·23
10·0	0·10	−0·24	0·15
∞	0·098	−0·25	0·14

TABLE 3

into (5.19) to obtain a pair of amplitude equations:

$$\nu_{01}\dot{A}_{01} = (M - M_c)\,A_{01} - Z_{01}, \tag{6.42}$$

$$\nu_{02}\dot{A}_{02} = (M - M_c - M_c^{-1}R_{02}f_{02})\,A_{02} - Z_{02}. \tag{6.43}$$

Using the formula (6.10), we find that

$$d_{01}Z_{01} = M(\gamma_{11}A_{01}^2 + \gamma_{112}A_{01}A_{02} + \gamma_{12}A_{02}^2), \tag{6.44}$$

$$d_{02}Z_{02} = M(\gamma_{21}A_{01}^2 + \gamma_{212}A_{01}A_{02} + \gamma_{22}A_{02}^2), \tag{6.45}$$

where

$$\gamma_{ik} = \langle \theta_{0i}^*(\mathbf{v}_{0k}\cdot\nabla)\,\theta_{0k} + Pr^{-1}\mathbf{v}_{0i}^*\cdot(\mathbf{v}_{0k}\cdot\nabla)\,\mathbf{v}_{0k}\rangle \tag{6.46}$$

for $i, k = 1, 2$, and

$$\gamma_{i12} = \langle \theta_{0i}^*(\mathbf{v}_{01}\cdot\nabla\theta_{02} + \mathbf{v}_{02}\cdot\nabla\theta_{01}) + Pr^{-1}\mathbf{v}_{0i}^*\cdot(\mathbf{v}_{01}\cdot\nabla\mathbf{v}_{02} + \mathbf{v}_{02}\cdot\nabla\mathbf{v}_{01})\rangle. \tag{6.47}$$

We approximate as before for M close to M_c, and on the assumption that the magnitude of A_{02} is much smaller than that of A_{01}. We then solve (6.43) and (6.45) to obtain

$$A_{02} = \frac{-M_c^2\gamma_{21}A_{01}^2}{R_{02}f_{02}d_{02}}. \tag{6.48}$$

We substitute this and (6.44) into (6.42), with M replaced by M_c in the nonlinear terms and with the terms containing A_{02}^2 omitted on the grounds that it is smaller than those retained. This leads to a single equation for the critical-mode amplitude, namely

$$\nu_{01}\dot{A}_{01} = (M - M_c)\,A_{01} - \gamma_0 A_{01}^2 - \omega_{01}A_{01}^3, \tag{6.49}$$

where

$$\gamma_0 = M_c\gamma_{11}/d_{01}, \tag{6.50}$$

$$\omega_{01} = \frac{-M_c^3\gamma_{21}\gamma_{112}}{R_{02}d_{01}d_{02}f_{02}}. \tag{6.51}$$

Computed values of the coefficients are given in table 3.

Observe that ν_{01}, ω_{01} are both positive, but that γ_0 is positive for low Prandtl numbers and negative for moderate and large Prandtl numbers.

One solution of (6.49) is $A_{01} = 0$, which corresponds to the conduction state. This solution is stable for $M < M_c$ and unstable for $M > M_c$. Other solutions are determined from roots of the equation

$$\omega_{01}A_{01}^2 + \gamma_0 A_{01} - (M - M_c) = 0. \tag{6.52}$$

All the solutions are illustrated in figure 4(*a*) for the case $\gamma_0 > 0$, and in figure 4(*b*) for the case $\gamma_0 < 0$. A convection solution exists for both $M < M_c$ and $M > M_c$ (trans-

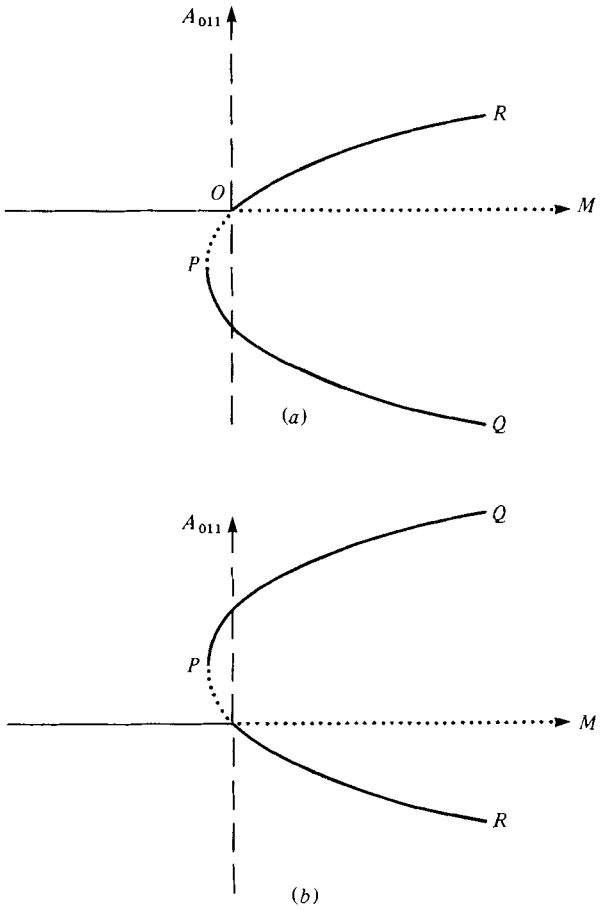

FIGURE 4. The bifurcation diagrams for $a = 1{\cdot}80$, corresponding to a pure axisymmetric mode $m = 0$. Solid lines represent stable branches while dotted lines represent unstable branches. (*a*) The case of $Pr = 0{\cdot}1$; the branch PQ represents downflow in the centre. (*b*) The case of $Pr \geqslant 1$; the branch PQ represents upflow in the centre.

critical bifurcation), but the subcritical branch turns around at a value M_0 of M and continues into the half-plane $M > M_c$.

We determine the stability of the solutions in the following way. Let $\bar{A}$ denote any time-independent solution of (6.49). We set

$$A_{01} = \bar{A} + a_0 \tag{6.53}$$

in equation (6.49) and linearize, to obtain the stability equation

$$\nu_{01}\dot{a}_0 = (M - M_c - 2\gamma_0\bar{A} - 3\omega_{01}\bar{A}^2)\,a_0 \tag{6.54}$$

A simple calculation shows that the subcritical branch OP in figure 4 is unstable, and that the branches OR, PQ are stable. This is the standard result for transcritical bifurcation.

These calculations settle in principle the question of the *direction of the flow at the centre of the container* because the asymmetry of the bifurcation diagram implies a preferred branch. As M increases towards M_c, a disturbance, however small, to the

conduction solution will result in loss of stability of the latter *before* M reaches the critical value M_c, and a consequent *snap-through* to the branch PQ. As M increases still further the system stays on the branch PQ, which is thus 'preferred' to the branch OR. Of course, when $M > M_c$ one could find a disturbance of large-enough size that would cause the system to jump from this branch to the other. The fact that *both* supercritical branches are stable is similar to the result of Liang, Vidal & Acrivos (1969) for axisymmetric buoyancy-driven convection in a cylinder.

From (5.6) we see that the vertical velocity component at the centre of the container for the mode 01 is

$$w_{01} = A_{01} Y_{01}(z). \tag{6.55}$$

Numerical calculations show that $Y_{01}(z) > 0$ on $0 < z < 1$; here the sign of A_{01} determines the direction of the flow, giving upflow when $A_{01} > 0$ and downflow when $A_{01} < 0$. The preferred branch PQ has $A_{01} < 0$ for very small Prandtl numbers and $A_{01} > 0$ for moderate and large Prandtl numbers. We infer that there will be downflow at the centre when $Pr \ll 1$, and upflow when $Pr > 1$.

7. Evolution at double points

It is evident from figures 1–3 that there are certain values of the aspect ratio at which two modes lose stability simultaneously. In this section we shall investigate the onset of convection in the neighbourhoods of such double points and the secondary bifurcations that can occur.

7.1. *Intersection of modes* 11, 21

At the point marked A in figure 1 the curves of M as a function of aspect ratio for the modes 11 and 21 intersect. The value of a at which this intersection takes place is denoted by a_A ($\simeq 1{\cdot}20$). The common value of M_{11}, M_{21} at this point will be denoted by M_c; computations give

$$M_c = M_{11} = M_{21} = 85{\cdot}2. \tag{7.1}$$

By hypothesis we have that $R_{11} = R_{21} = 0$.

We are interested in studying the onset of convection at values of a slightly less and slightly greater than a_A. As noted in § 6, the self-interaction of the mode 11 generates modes with azimuthal wavenumbers 0 and 2, while the self-interaction of the mode 21 generates modes with $m = 0$ and $m = 4$. In addition, the interaction of modes 11 and 21 generates a mode with $m = 3$. For reasons indicated earlier, we approximate by retaining only the leading (in the sense of eigenvalue ordering) member of each of these generated sets. This leads us to select a 5-element set of expansion functions, namely

$$\mathscr{S} = \{11, 21, 01, 31, 41\}. \tag{7.2}$$

Substituting the appropriate eigenfunction expansion into (5.19), we obtain a system of five ordinary differential equations for the amplitudes. These equations are conveniently written as follows:

$$\nu_{m1} \dot{A}_{m1} = (M - M_{m1}) A_{m1} - Z_{m1} \quad (m = 1, 2), \tag{7.3}$$

$$\nu_{m1} \dot{A}_{m1} = (M - M_c^{-1} R_{m1} f_{m1}) A_{m1} - Z_{m1} \quad (m = 0, 3, 4). \tag{7.4}$$

Note that in (7.3) we have retained M_{m1} in place of M_c; the reason for this will soon become apparent.

We reduce the system (7.3), (7.4) as in § 6. We use (6.10) to calculate the quadratic nonlinearities in (7.4), and find

$$d_{01}Z_{01} = M(\alpha_{01}A_{11}^2 + \alpha_{02}A_{21}^2 + \alpha_{00}A_{01}^2 + \alpha_{03}A_{31}^2 + \alpha_{04}A_{41}^2), \tag{7.5a}$$

$$d_{31}Z_{31} = M\alpha_{312}A_{11}A_{21}, \tag{7.5b}$$

$$d_{41}Z_{41} = M(\alpha_{42}A_{21}^2 + \beta_{404}A_{01}A_{41} + \alpha_{413}A_{11}A_{31}), \tag{7.5c}$$

where the α_{mk} are given by (6.16), β_{404} is given by (6.34), and where

$$\alpha_{mjk} = \langle \theta_{m1}^*(\mathbf{v}_{j1}.\nabla\theta_{k1} + \mathbf{v}_{k1}.\nabla\theta_{j1}) + Pr^{-1}\mathbf{v}_{m1}^*.(\mathbf{v}_{j1}.\nabla\mathbf{v}_{k1} + \mathbf{v}_{k1}.\nabla\mathbf{v}_{j1})\rangle. \tag{7.6}$$

We now solve (7.4) approximately by neglecting the time-derivative terms, replacing M by M_c, and neglecting as relatively small the quadratic terms involving A_{01}, A_{31} and A_{41} on the right-hand sides of (7.5*a–c*). This process gives the approximations

$$\left.\begin{aligned} A_{01} &= \frac{-M_c^2}{R_{01}f_{01}d_{01}}(\alpha_{01}A_{11}^2 + \alpha_{02}A_{21}^2), \\ A_{41} &= \frac{-M_c^2\alpha_{42}A_{21}^2}{R_{41}f_{41}d_{41}}, \quad A_{31} = \frac{-M_c^2\alpha_{312}A_{11}A_{21}}{R_{31}f_{31}d_{31}}. \end{aligned}\right\} \tag{7.7}$$

These formulae can be compared with (6.18) and (6.35), it being noted in particular that $\alpha_{02} = \beta_{02}$ and $\alpha_{42} = \beta_{42}$.

The quadratic nonlinearities in (7.3) are found to be given by

$$d_{11}Z_{11} = MA_{11}(\alpha_0 A_{01} + \alpha_2 A_{21}) + M\alpha_{123}A_{21}A_{31}, \tag{7.8}$$

$$d_{21}Z_{21} = M(\alpha_{21}A_{11}^2 + \beta_0 A_{21}A_{01} + \beta_4 A_{21}A_{41} + \alpha_{213}A_{11}A_{31}), \tag{7.9}$$

where α_0, α_2 are defined by (6.13), α_{21} by (6.16), β_0, β_4 by (6.30), and $\alpha_{213}, \alpha_{123}$ by (7.6). We now substitute (7.7)–(7.9) into (7.3) to obtain the following pair of equations:

$$\nu_{11}\dot{A}_{11} = (M - M_{11})A_{11} - c_1 A_{11}A_{21} - \omega_1 A_{11}^3 - \sigma_1 A_{11}A_{21}^2, \tag{7.10}$$

$$\nu_{21}\dot{A}_{21} = (M - M_{21})A_{21} - c_2 A_{11}^2 - \sigma_2 A_{11}^2 A_{21} - \omega_2 A_{21}^3, \tag{7.11}$$

where the coefficients are defined by the following formulae:

$$\left.\begin{aligned} c_1 &= M_c\alpha_2/d_{11}, \quad c_2 = M_c\alpha_{21}/d_{21}, \\ \sigma_1 &= \frac{-M_c^3}{d_{11}}\left\{\frac{\alpha_0\alpha_{02}}{R_{01}f_{01}d_{01}} + \frac{\alpha_{123}\alpha_{312}}{R_{31}f_{31}d_{31}}\right\}, \\ \sigma_2 &= \frac{-M_c^3}{d_{21}}\left\{\frac{\beta_0\alpha_{01}}{R_{01}f_{01}d_{01}} + \frac{\alpha_{213}\alpha_{312}}{R_{31}f_{31}d_{31}}\right\}, \\ \omega_1 &= \frac{-M_c^3\alpha_0\alpha_{01}}{R_{01}f_{01}d_{01}d_{11}}, \quad \omega_2 = \omega_{21}, \end{aligned}\right\} \tag{7.12}$$

and where ω_{21} is defined by (6.37). Computed values of the coefficients are given in table 4.

We propose to study the nature and stability of solutions of (7.10), (7.11) in the neighbourhood of the double point A, and for values of M reasonably close to M_c.

Pr	$\nu_{11}\times10^{-4}$	$c_1\times10^{-2}$	$\omega_1\times10^{-2}$	$\sigma_1\times10^{-3}$	$\nu_{21}\times10^{-3}$	$c_2\times10^{-2}$	$\sigma_2\times10^{-3}$	$\omega_2\times10^{-2}$
0·1	0·49	−1·2	14·0	2·0	3·7	1·3	1·6	4·2
1·0	0·19	−0·74	1·5	0·27	1·2	0·36	0·28	0·62
10·0	0·16	−0·69	0·93	0·18	0·91	0·26	0·20	0·31
∞	0·16	−0·69	0·88	0·17	0·89	0·25	0·19	0·28

TABLE 4

We consider first the case of *aspect ratios slightly less than* a_A, $a < a_A$. We then have that

$$M_{11} < M_{21}, \tag{7.13}$$

and we define

$$\eta = M - M_{11}, \quad \Delta = M_{21} - M_{11}. \tag{7.14}$$

Equations (7.10), (7.11) can now be written in the form

$$\left.\begin{aligned} \nu_1 \dot{A}_1 &= \eta A_1 - c_1 A_1 A_2 - \omega_1 A_1^3 - \sigma_1 A_1 A_2^2, \\ \nu_2 \dot{A}_2 &= (\eta - \Delta) A_2 - c_2 A_1^2 - \sigma_2 A_1^2 A_2 - \omega_2 A_2^3, \end{aligned}\right\} \tag{7.15}$$

where for the sake of brevity the notation has been simplified in an obvious way.

Because of the approximations used in their derivation, the equations (7.15) can be regarded as valid only for small values of Δ and small values of η. A reasonable measure of smallness is the ratio of these quantities to the critical value of M, which is about 85. In the computations to be described presently we have taken values of Δ in the range $0 \leqslant \Delta \leqslant 5{\cdot}0$ and values of η in the range $0 \leqslant \eta \leqslant 2\Delta$. Results for significantly larger values are not easily substantiated on the basis of our approximation scheme.

Before proceeding further we formulate the stability problem associated with the system (7.15). Let $(\bar{A}_1, \bar{A}_2)$ denote a solution of (7.15) and set

$$A_1 = \bar{A}_1 + a_1, \quad A_2 = \bar{A}_2 + a_2. \tag{7.16}$$

Linearization of the equations with respect to the disturbances leads to the linear system

$$\left.\begin{aligned} \nu_1 \dot{a}_1 &= (\eta - c_1 \bar{A}_2 - 3\omega_1 \bar{A}_1^2 - \sigma_1 \bar{A}_2^2) a_1 - (c_1 + 2\sigma_1 \bar{A}_2) \bar{A}_1 a_2, \\ \nu_2 \dot{a}_2 &= -2(c_2 + \sigma_2 \bar{A}_2) \bar{A}_1 a_1 + (\eta - \Delta - \sigma_2 \bar{A}_1^2 - 3\omega_2 \bar{A}_2^2) a_2. \end{aligned}\right\} \tag{7.17}$$

The exponents of this system determine the stability of the solution $(\bar{A}_1, \bar{A}_2)$.

We examine now the solutions of (7.15) and their stability. Observe first that (7.15) has the trivial solution $A_1 = A_2 = 0$, which corresponds to the conduction state, and which is stable for $\eta < 0$ and unstable for $\eta > 0$. Moreover, for this solution one stability exponent changes sign at $\eta = 0$ and the other at $\eta = \Delta$, so that each of these values locates a bifurcation point for the appearance of a new (convection) solution.

The trivial solution is unique for $\eta < 0$. As η increases through zero, a pair of non-trivial solutions emerges, determined by the pair of equations

$$\left.\begin{aligned} A_1^2 &= (\eta - c_1 A_2 - \sigma_1 A_2^2)/\omega_1, \\ \omega_2 A_2^3 + \sigma_2 A_1^2 A_2 + c_2 A_1^2 - (\eta - \Delta) A_2 &= 0. \end{aligned}\right\} \tag{7.18}$$

If Δ were large, these equations would reduce to $A_2 = 0$ and A_1 (equivalent to A_{111})

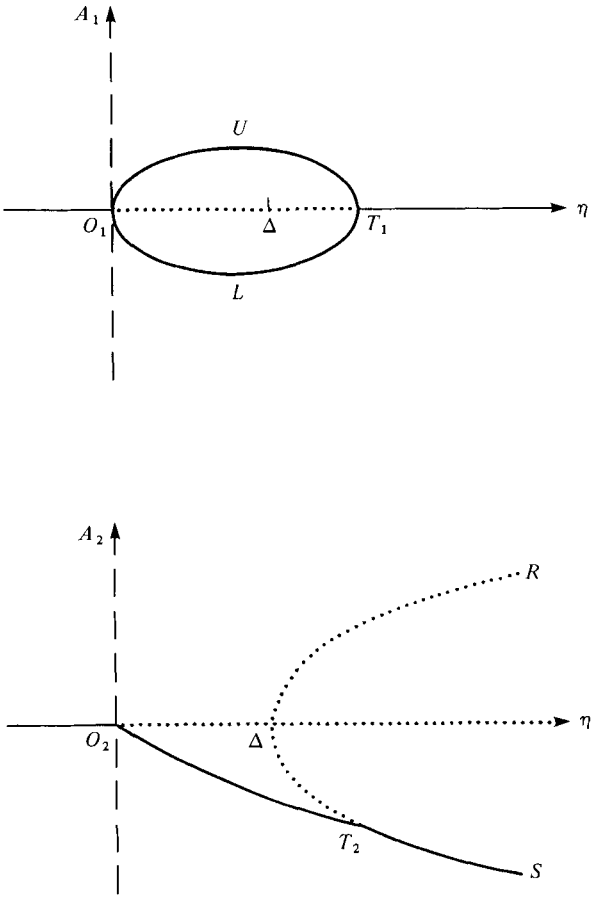

FIGURE 5. The bifurcation diagrams for a slightly less than $a_A \simeq 1{\cdot}20$, where $\Delta = M_{21} - M_{11}$. Solid lines represent stable branches while dotted lines represent unstable branches.

given by (6.22), and would correspond to a 'pure' convection state with azimuthal wavenumber $m = 1$ at leading order. When Δ is small, however, the mode $m = 2$ has an effect, as expressed by the coupled equations (7.18), in two ways: the solution has $A_2 \neq 0$ and the parabolas (6.22) are distorted as η approaches Δ.

Numerical calculations show that solutions of (7.18) exist only on an interval $0 < \eta < \eta_T$, where $\eta_T > \Delta$. The value of η_T depends on Prandtl number, but computations reveal that $1 < \eta_T/\Delta \leqslant 1{\cdot}2$ for the entire Prandtl-number range. On $0 < \eta < \eta_T$ there is precisely one root $\bar{A}_2$ of the cubic in (7.18), and a corresponding pair of roots $+\bar{A}_1, -\bar{A}_1$. These solutions are illustrated in figure 5: one pair of solutions is represented by the curves $O_1 UT_1, O_2 T_2$ and the other by the curves $O_1 LT_1, O_2 T_2$.

Calculations utilizing (7.17) show that these solutions are *stable*.

The remaining solutions of (7.15) are given by

$$A_1 \equiv 0, \quad \eta - \Delta = \omega_2 \bar{A}_2^2. \tag{7.19}$$

These exist for $\eta > \Delta$ and are the 'pure' $m = 2$ mode solutions considered in § 6.2. Their stability is determined by substituting (7.19) into (7.17), which gives

$$\nu_1 \dot{a}_1 = (\eta - c_1 \bar{A}_2 - \sigma_1 \bar{A}_2^2) a_1, \quad \nu_2 \dot{a}_2 = -2(\eta - \Delta) a_2. \tag{7.20}$$

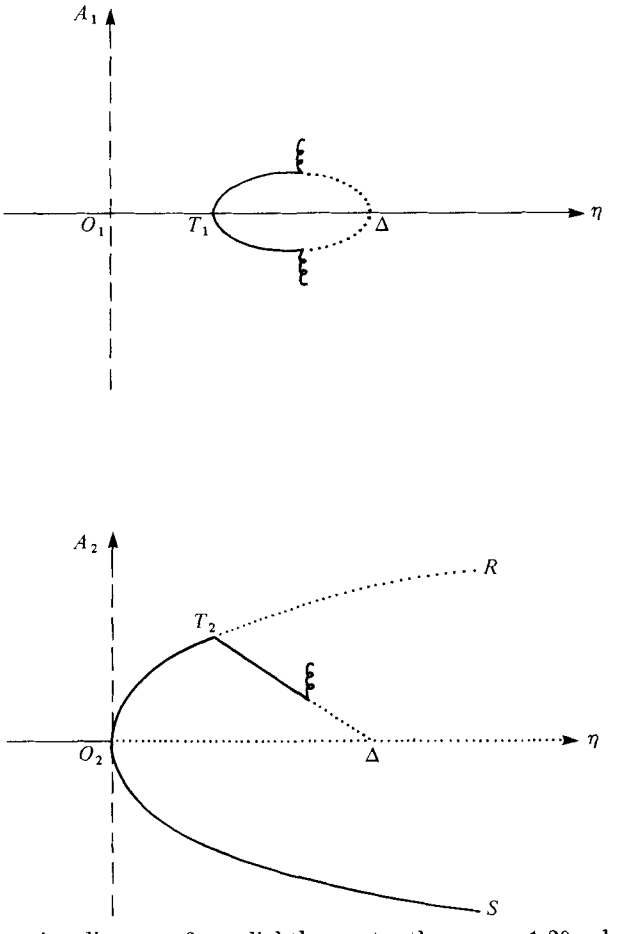

FIGURE 6. The bifurcation diagrams for a slightly greater than $a_A \simeq 1{\cdot}20$, where $\Delta = M_{11} - M_{21}$. Solid lines represent stable branches while dotted lines represent unstable branches. The curly lines represent time-periodic bifurcations. The orientations of these branches and their stability properties are unknown.

Evidently it is the first of these equations that decides stability. Calculations show that the branch corresponding to positive $\bar{A}_2$, the upper branch ΔR in figure 5, is unstable, while the lower branch, ΔS, is unstable initially but regains stability at precisely the value $\eta = \eta_T$ defined above.

The situation depicted in figure 5 has been established numerically. In summary, the behaviour of the system is as follows. For $\eta < 0$ ($M < M_{11}$) the conduction solution is stable, and is replaced on $0 < \eta < \eta_T$ ($M_{11} < M < M_T$, say) by a pair of mixed-mode solutions given by (7.18). For $\eta > \eta_T$, however, these give way to a single solution which at leading order is a pure convective state with $m = 2$. This behaviour is qualitatively independent of Prandtl number.

For aspect ratios slightly greater than a_A, $a > a_A$, we have

$$M_{21} < M_{11}. \tag{7.21}$$

We then set

$$\eta = M - M_{21}, \quad \Delta = M_{11} - M_{21} \tag{7.22}$$

to obtain the system

$$\left.\begin{aligned} \nu_1 \dot{A}_1 &= (\eta-\Delta)A_1 - c_1 A_1 A_2 - \omega_1 A_1^3 - \sigma_1 A_1 A_2^2, \\ \nu_2 \dot{A}_2 &= \eta A_2 - c_2 A_1^2 - \sigma_2 A_1^2 A_2 - \omega_2 A_2^3. \end{aligned}\right\} \tag{7.23}$$

The stability equations for a solution $(\bar{A}_1, \bar{A}_2)$ of this system are similar to (7.17), except that the terms η and $\eta-\Delta$ are interchanged.

The results of numerical calculations for (7.23), illustrated in figure 6, are as follows. The conduction solution $A_1 = A_2 = 0$ exists for all η, and is stable for $\eta < 0$ and unstable for $\eta > 0$. The solutions defined by

$$A_1 = 0, \quad A_2^2 = \bar{A}_2^2 = \eta/\omega_2 \tag{7.24}$$

exist for $\eta > 0$. The lower branch O_2S is always stable, while the upper branch is stable for $0 < \eta < \eta_T$, where $\eta_T \in (0, \Delta)$, and has a value dependent on Prandtl number. The solutions determined by

$$\left.\begin{aligned} A_1^2 &= (\eta-\Delta-c_1 A_2 - \sigma_1 A_2^2)/\omega_1, \\ \omega_2 A_2^3 &+ \sigma_2 A_1^2 A_2 + c_2 A_1^2 - \eta A_2 = 0 \end{aligned}\right\} \tag{7.25}$$

exist on the interval $\eta_T < \eta < \Delta$. There are two such solutions, comprising a single root A_2 and corresponding $\pm A_1$. These solutions are found to be stable for $\eta < \eta_s$. They become unstable at $\eta = \eta_s$ to time-periodic disturbances, so that the curly line in figure 6 denotes a Hopf bifurcation.

We see from figure 6 that the conduction solution is replaced by the pair of solutions (7.24) on $0 < \eta < \eta_T$. Next, there is a region, $\eta_T < \eta < \eta_s$, in which there are three stable solutions: the lower branch of (7.24) and the mixed-mode solutions of (7.25). When $\eta_s < \eta < \Delta$, the pure mode O_2S is stable. We have *not tested* the stability of the time-periodic Hopf solutions. However, for $\eta > \Delta$ there is only one (stable) steady solution, which is a pure non-axisymmetric mode with $m = 2$. These results apply at all Prandtl numbers.

We see from figures 5 and 6, and from the preceding discussions, that on either side of the aspect ratio a_A the system may eventually attain the same state: a pure convection solution with $m = 2$, so that one way or another the mode with $m = 1$ is suppressed by the interaction when Δ is small. This interaction can therefore be regarded as being a mechanism for wavenumber selection in the sense just described. Of course, for $a > a_A$, there may be a time-periodic mode that ultimately survives.

7.2. *Intersection of modes* 21, 01

The point B in figure 1 is the intersection of the curves for the modes 21 and 01. We denote the corresponding value of a by a_B ($\simeq 1{\cdot}70$). The common value of M_{21}, M_{01} at this point will be denoted by M_c; computations give

$$M_c = M_{21} = M_{01} = 80{\cdot}6. \tag{7.26}$$

By hypothesis we have that $R_{21} = R_{01} = 0$. Using the same reasoning as in the previous case, we take

$$\mathscr{S} = \{21, 01, 41, 02\} \tag{7.27}$$

as the set of eigenfunctions for the evolution of the modes 21 and 01 near the double point.

Substituting the associated eigenfunction expansion into (5.19), we obtain, by analogy with (7.3) and (7.4), the following ordinary differential equations:

$$\nu_{m1}\dot{A}_{m1} = (M - M_{m1})A_{m1} - Z_{m1} \quad (m = 2, 0), \tag{7.28}$$

$$\nu_{mi}\dot{A}_{mi} = (M - M_c - M_c^{-1}R_{mi}f_{mi})A_{mi} - Z_{mi} \quad (m = 4, \quad i = 1 \quad \text{and} \quad m = 0, \quad i = 2). \tag{7.29}$$

For the quadratic nonlinearities in (7.29) we use (6.10) to find that

$$d_{41}Z_{41} = M(\beta_{42}A_{21}^2 + \beta_{404}A_{01}A_{41} + \bar{\beta}_{404}A_{02}A_{41}), \tag{7.30}$$

where β_{42} is given by (6.33), β_{404} by (6.34) and $\bar{\beta}_{404}$ by (6.34) with the mode 011 replaced by the mode 021. Here

$$d_{02}Z_{02} = M(\delta_{22}A_{21}^2 + \gamma_{21}A_{01}^2 + \gamma_{212}A_{01}A_{21} + \gamma_{22}A_{02}^2 + \delta_{24}A_{41}^2), \tag{7.31}$$

where the γ are given by (6.46), (6.47), and we define

$$\delta_{km} = \langle \theta_{0k}^*(\mathbf{v}_{m1}\cdot\nabla)\theta_{m1} + Pr^{-1}\mathbf{v}_{0k}^*\cdot(\mathbf{v}_{m1}\cdot\nabla)\mathbf{v}_{m1}\rangle \tag{7.32}$$

for $k = 1, 2$ and $m = 2, 4$. We now solve (7.29), making the same approximations as before, to obtain

$$A_{02} = \frac{-M_c^2}{R_{02}f_{02}d_{02}}(\delta_{22}A_{21}^2 + \gamma_{21}A_{01}^2), \quad A_{41} = \frac{-M_c^2\beta_{42}A_{21}^2}{R_{41}f_{41}d_{41}}. \tag{7.33}$$

The quadratic nonlinearities in (7.27) are found to be given by

$$d_{21}Z_{21} = MA_{21}(\beta_0 A_{01} + \bar{\beta}_0 A_{02} + \beta_4 A_{41}), \tag{7.34}$$

where β_0, β_4 are given by (6.30), and $\bar{\beta}_0$ is also defined by (6.30) with 01 replaced by 02. Here

$$d_{01}Z_{01} = M(\gamma_{11}A_{01}^2 + \gamma_{112}A_{01}A_{02} + \gamma_{12}A_{02}^2 + \delta_{12}A_{21}^2 + \delta_{14}A_{41}^2), \tag{7.35}$$

where the γ are given by (6.46), (6.47) and the δ by (7.31).

We now substitute (7.33)–(7.35) into (7.28) to obtain the following pair of equations:

$$\left.\begin{aligned} \nu_{21}\dot{A}_{21} &= (M - M_{21})A_{21} - c_2 A_{21}A_{01} - \sigma_2 A_{21}A_{01}^2 - \omega_2 A_{21}^3, \\ \nu_{01}\dot{A}_{01} &= (M - M_{01})A_{01} - \gamma_0 A_{01}^2 - c_0 A_{21}^2 - \sigma_0 A_{01}A_{21}^2 - \omega_0 A_{01}^3, \end{aligned}\right\} \tag{7.36}$$

where

$$\left.\begin{aligned} c_2 &= M_c\beta_0/d_{21}, \quad c_0 = M_c\delta_{12}/d_{01}, \\ \sigma_2 &= \frac{-M_c^3\bar{\beta}_0\gamma_{21}}{R_{02}d_{02}f_{02}d_{21}}, \quad \sigma_0 = \frac{-M_c^3\delta_{22}\gamma_{112}}{R_{02}d_{02}f_{02}d_{01}}, \\ \omega_2 &= -\frac{M_c^3}{d_{21}}\left(\frac{\bar{\beta}_0\delta_{22}}{R_{02}d_{02}f_{02}} + \frac{\beta_4\beta_{42}}{R_{41}d_{41}f_{41}}\right), \end{aligned}\right\} \tag{7.37}$$

where $\omega_0 = \omega_{01}$ (defined by (6.51)), and γ_0 is given by (6.50). Computed values of the coefficients are given in table 5. Notice that the values of c_0 are quite small in magnitude, and hence are potentially subject to relatively large truncation errors.

We proceed with the analysis as in the previous case. For *aspect ratios slightly less than* a_B, $a < a_B$, we define

$$\eta = M - M_{21}, \quad \Delta = M_{01} - M_{21} > 0, \tag{7.38}$$

whereupon the equations (7.36) become

$$\left.\begin{aligned} \nu_2\dot{A}_2 &= \eta A_2 - c_2 A_2 A_0 - \sigma_2 A_2 A_0^2 - \omega_2 A_2^3, \\ \nu_0\dot{A}_0 &= (\eta - \Delta)A_0 - \gamma_0 A_0^2 - c_0 A_2^2 - \sigma_0 A_0 A_2^2 - \omega_0 A_0^3, \end{aligned}\right\} \tag{7.39}$$

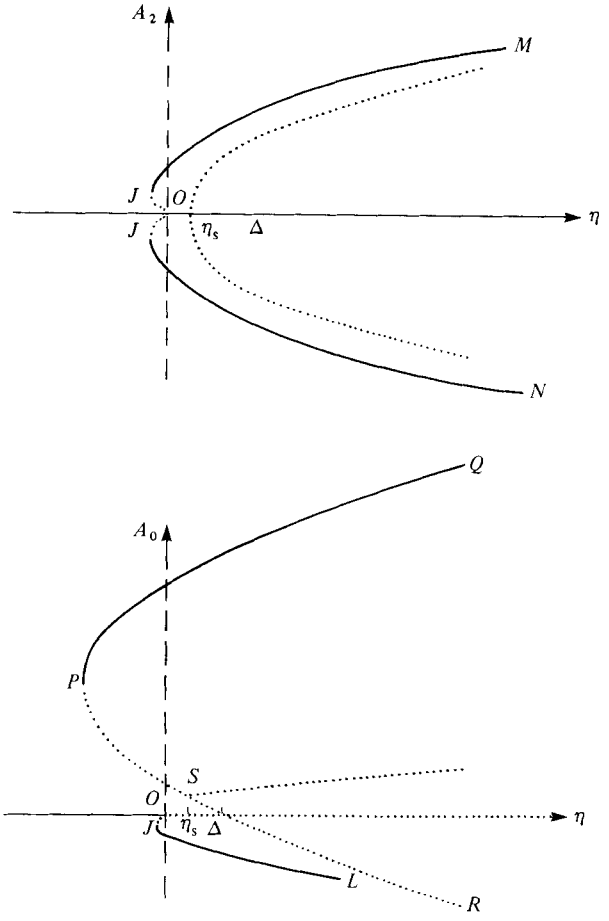

FIGURE 7. The bifurcation diagrams for $Pr = 10$ and ∞ for a slightly less than $a_B \simeq 1{\cdot}70$, where $\Delta = M_{01} - M_{21}$. Solid lines represent stable branches while dotted lines represent unstable branches.

with an obvious abbreviated notation. The stability problem for a solution $(\bar{A}_2, \bar{A}_0)$ of (7.39) is determined from the equations

$$\left.\begin{aligned} \nu_2 \dot{a}_2 &= (\eta - c_2\bar{A}_0 - \sigma_2\bar{A}_0^2 - 3\omega_2\bar{A}_2^2)a_2 - (c_2\bar{A}_2 + 2\sigma_2\bar{A}_2\bar{A}_0)a_0, \\ \nu_0 \dot{a}_0 &= -(2c_0\bar{A}_2 + 2\sigma_0\bar{A}_0\bar{A}_2)a_2 + (\eta - \Delta - 2\gamma_0\bar{A}_0 - 3\omega_0\bar{A}_0^2)a_0. \end{aligned}\right\} \tag{7.40}$$

The solutions of (7.39) and their stability behaviour are locally sensitive to the signs of the constants γ_0 and c_0 in table 5, and hence to variation in Prandtl number. The behaviour for large Prandtl number is illustrated in figure 7. The conduction solution $A_2 = A_0 = 0$ loses stability at $\eta = 0$, and the solution that bifurcates from this point is primarily an $m = 2$ mode, modified by the presence of a small $m = 0$ component. The latter is due to the fact that (7.39) have no non-trivial solutions with $A_0 = 0$, owing to the presence of the term $c_0 A_2^2$. This solution is represented by the curves OM, ON, OL in figure 7, and derives from the equations

$$\left.\begin{aligned} A_2^2 &= (\eta - c_2 A_0 - \sigma_2 A_0^2)/\omega_2, \\ 0 &= (\eta - \Delta)A_0 - \gamma_0 A_0^2 - c_0 A_2^2 - \sigma_0 A_0 A_2^2 - \omega_0 A_0^3. \end{aligned}\right\} \tag{7.41}$$

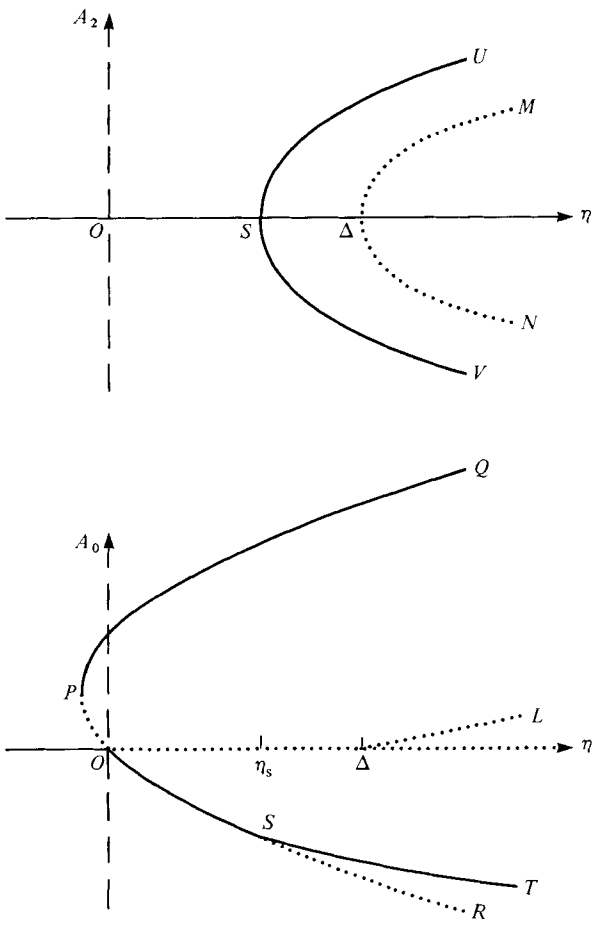

FIGURE 8. The bifurcation diagrams for $Pr = 10$ and ∞ for a slightly greater than $a_B \simeq 1{\cdot}70$, where $\Delta = M_{21} - M_{11}$. Solid lines represent stable branches while dotted lines represent unstable branches.

This solution is initially subcritical, but quickly turns around at the point J. The branches to the right of J are stable.

The solution bifurcating at the point $\eta = \Delta$ is given by

$$A_2 = 0, \quad \eta - \Delta - \gamma_0 A_0 - \omega_0 A_0^2 = 0. \tag{7.42}$$

This is identical with the transcritical solution described in § 6.3, and is represented by the asymmetrical parabola QPR. However, the stability system shows that the branch PQ is stable (as in figure 4), but that the whole branch PR is now unstable.

In particular we find that there is a value η_s of η, with $0 < \eta_s < \Delta$, at which one of the stability exponents for the branch PR changes sign. From the corresponding point S on PR there is secondary bifurcation into a mixed-mode solution. This is actually a distinct solution of the equations (7.40), and is unstable.

Reviewing the situation as shown in figure 7, we see that, well before η reaches 0, the system is likely to snap through to the axisymmetric branch PQ; otherwise, if it reaches close to O, it will eventually end up on the predominantly $m = 2$ solution OM, ON, OL.

Pr	$\nu_{21}\times10^{-4}$	$c_2\times10^{-1}$	$\sigma_2\times10^{-2}$	$\omega_2\times10^{-2}$	$\nu_{01}\times10^{-3}$	$\gamma_0\times10^{-2}$	c_0	$\sigma_0\times10^{-2}$	$\omega_0\times10^{-3}$
0·1	0·40	0·22	6·9	11·0	3·6	0·36	−19·0	1·6	1·7
1·0	0·15	4·3	0·55	1·5	1·2	−0·21	− 1·4	0·22	0·21
10·0	0·12	4·7	0·30	0·98	0·96	−0·26	0·40	0·15	0·14
∞	0·12	4·8	0·28	0·94	0·94	−0·27	0·57	0·14	0·13

TABLE 5

Thus, even though the $m = 2$ mode appears first according to linear theory, it is less likely to be selected than the axisymmetric mode.

For Prandtl numbers $Pr = 0{\cdot}1$ and $1{\cdot}0$ the interactions are different near the bifurcation points; the secondary branch emerging from $\eta = \eta_s$ opens to the left and joins with the solution out of $\eta = 0$. Thus, a closed loop in A_2 appears, analogous to that shown in figure 6. Similarly, the loop loses stability to time-periodic bifurcations whose orientation and stability are unknown. Again, we find that the axisymmetric mode emerges as the likely preferred mode when $\eta > 0$.

We consider next the case where a is slightly greater than a_B, $a > a_B$, with

$$\eta = M - M_{01}, \quad \Delta = M_{21} - M_{01} > 0. \tag{7.43}$$

The governing equations are (7.39) with η and $\eta - \Delta$ interchanged, and the stability equations are (7.40) with η and $\eta - \Delta$ interchanged. The results again vary with Prandtl number, and the cases for $Pr = 10$ and ∞ are shown in figure 8.

The solution bifurcating from $\eta = 0$ is the transcritical axisymmetric solution given by

$$A_2 = 0, \quad \eta - \gamma_0 A_0 - \omega_0 A_0^2 = 0, \tag{7.44}$$

represented by the curves PQ, PR in figure 8. Calculations based on (7.40) show that the branch PQ is stable and PO is unstable, as in the non-interactive case depicted in figure 4, but that OR, initially stable, loses stability at $\eta = \eta_s$, where $0 < \eta_s < \Delta$. This re-emphasizes the preference for the upper branch, discussed in § 8.

The solution bifurcating from $\eta = \Delta$ is a solution of the equations

$$\left.\begin{aligned} A_2^2 &= (\eta - \Delta - c_2 A_0 - \sigma_2 A_0^2)/\omega_2, \\ 0 &= \eta A_0 - \gamma_0 A_0^2 - c_0 A_2^2 - \sigma_0 A_0 A_2^2 - \omega_0 A_0^3. \end{aligned}\right\} \tag{7.45}$$

It is found to exist for $\eta > \Delta$ and to be a slight modification of the pure $m = 2$ solution described in § 6.2. This solution is represented by the curves ΔL, ΔM and ΔN in figure 8. Calculations show it to be unstable.

Finally, there is another solution of (7.45), which is a mixed mode and which bifurcates from the axisymmetric solution (7.44) at the point S. This solution is represented by the curves SU, SV, ST in figure 8, and is found to be stable.

We see, therefore, that there are two stable solutions: the pure axisymmetric mode PQ, and the mixed mode emanating from S. The latter represents a distortion of the lower branch due to the modal interaction. Nevertheless the upper branch PQ is preferred, as in the non-interactive situation.

For $Pr = 1{\cdot}0$ the branch QPR remains as it is, but for $Pr = 0{\cdot}1$ it becomes reflected in the η-axis. The portion PQ of this branch remains preferred since branch $M\Delta N$ inverts and connects up with USV to form a closed loop.

8. Discussion and conclusions

We have considered Marangoni instability in a circular cylinder under the simplifying assumptions that the upper free surface is non-deformable, i.e. $C \to 0$, and the side walls are adiabatic and impenetrable but 'slippery'.

The linear stability curves vary with surface Biot number L and Rayleigh number R as expected from the analyses of the unbounded layer, since the underlying eigenvalue problems are identical. M_c decreases with R and increases with L; these features are shown in figures 1–3. Here, the envelope of each set of curves gives M_c for each aspect ratio. Had we used the more-realistic rigid-side-wall boundary conditions, this envelope would have been modified. We would still expect to have interlacing of the modes, though the modes might interlace in a different sequence. Only the direct calculation of these neutral stability curves could determine this. We shall discuss below the implications of the use of slippery side-wall conditions.

Given the qualitative similarities of cases for various values of L and R, we have investigated the nonlinear behaviour only for the single set $L = 0$, $R = 0$. We have selected five aspect ratios and performed the bifurcation analyses for these.

The cases in §§ 6.1, 6.2 and 6.3 relate to aspect ratios corresponding to simple eigenvalues M_c for which $m = 1, 2, 0$, respectively. We see that for $m \neq 0$ that we have supercritical bifurcation only. However, when $m = 0$, the axisymmetric convection is subcritical, and snap-through convection can be expected. It is only in this axisymmetric case that the flow direction is distinguished. For low Prandtl number Pr, there is downflow in the centre, while for all $Pr \geqslant 1$ there is upflow in the centre. As is well-known, subcritical instabilities have associated transport values with hysteresis behaviour. It is easy to calculate the degree of subcriticality possible in the axisymmetric mode, i.e. the value of $\Delta M/M_c$ at the nose of the curve. This varies from 0·18 % at $Pr = 0{\cdot}1$ to 1·4 % at $Pr = \infty$. The only comparison available is with the results of Scanlon & Segel (1967), who examined an 'infinitely deep' layer having no side walls. In their analysis they had $Pr = \infty$ and found $\Delta M/M_c = 2{\cdot}3$ %. The two analyses are in reasonable agreement. This gives further substance to our feeling that our results reflect the inherent nonlinear behaviour of the system.

The case dealt with in § 7.1 examines a neighbourhood of $a = a_A$ of figure 1 where M_c is a double eigenvalue of modes $m = 1$ and 2. The nonlinear theory gives a coupled pair of nonlinear amplitude equations (7.15). The analysis shows (figure 6) that for a slightly larger than a_A the first mode to appear (at $M = M_c$) is the pure mode $m = 2$, as predicted by linear theory. As M is increased above M_c, the system remains in this mode, and possibly no further transition is predicted. Alternatively, the system may progress through the sequence: pure $m = 2$, mixed (1, 2), mixed time-periodic, and perhaps pure $m = 2$, as discussed in § 7. On the other hand, if a is slightly smaller than a_A the transition sequence (figure 5) is completely different. Here, at $M = M_c$, a mixed (1, 2) mode occurs, and this mode becomes unstable for an $M > M_c$. Hence there must be a transition to the pure mode $m = 2$. We find then that the mode $m = 2$ may persist and be stable for M large enough on either side of $a = a_A$ *independent of the prediction of linear theory.* This result depends on the stability of the time-periodic mode, which has not been examined here but will be investigated further in later work.

The case dealt with in § 7.2 examines a neighbourhood of $a = a_B$ of figure 1 where

M_c is a double eigenvalue of modes $m = 2$ and 0. The nonlinear theory gives a coupled pair of nonlinear amplitude equations (7.36). The analysis for $Pr = 10$ and ∞ shows (figure 8) that for a slightly larger than a_B the first mode to appear (at $M = M_c$) is the pure axisymmetric one. There is a snap-through at some $M < M_c$ (the snap-through is accompanied by a dynamical hysteresis behaviour). With sufficiently small disturbances the system resides in this $m = 0$ mode for all M covered by the theory. Yet, for M large enough there can be a transition to the mixed (2, 0) mode if the disturbances are large enough. On the other hand, if a is slightly smaller than a_B (figure 7) very small disturbances snap through to a mixed (2, 0) mode that is stable. There could be a snap-through transition (for large disturbances) to the pure $m = 0$ mode. If M is then decreased, a dynamical hysteresis loop would be revealed, since the jump back to the mixed mode would usually occur at much lower values of M; conceivably in fact, the jump could be to the state of pure conduction. This interesting hysteresis loop could consist of *three* distinct states: mixed (2, 0), pure $m = 0$, pure conduction. Alternatively, if the system is very noisy in that large disturbances are present, as M is increased from subcritical condition, the system could snap through directly from conduction (at $M < M_c$) to the axisymmetric state, and completely by-pass the mixed-mode state for increasing M, yet return to it when M is decreased.

If the Prandtl number is $Pr = 0{\cdot}1$ or $1{\cdot}0$, the situation is different. The mixed mode is always supercritical, and the pure $m = 0$ mode is encountered first and is stable.

The above analysis should give a faithful representation of the nonlinear processes in fairly small containers in which Marangoni instability takes place. If the replacing of the ideal side walls with more realistic rigid walls does not change the sequence of the modal interlacings, then the theory could be applied to experiment in a straightforward way. *If* the sequence of modal interlacings *does* change, then the theory should be applied by first locating the double eigenvalue by experimental observation. The location $a = a_B$, say, would be different from that of the 'slippery' wall linearized analysis. However, once it is located, the raising of M for aspect ratios a on either side of a_B might be well represented by the above theory. It is thus a relatively simple observation of flow pattern that would initially need verification.

There has been no previous nonlinear analysis of Marangoni convection in a bounded container. The present work represents a first exploration of the phenomena, albeit with an idealized model. The idealization on the upper free surface, $C \to 0$, will be removed in our future work so that effects of free-surface deflection can be assessed. The dropping of idealization of slippery side walls entails a major computing program that will not be undertaken. Clearly, certain small imperfections on either the side walls or the free surface can lead to an imperfect bifurcation in which the predicted sharp instabilities become gradual changes. Our work here provides the framework for studying these effects as well.

This work was supported by NASA–Lewis Research Center through Contract no. NAS3-22274. The authors are indebted to Dr P. H. Steen for valuable criticisms of an earlier version of the analysis.

Appendix

The eigenfunctions $X(z)$, $Y(z)$ satisfy a system derived from the linearized equations (4.3), (4.4), the boundary conditions (4.5), (4.6), and the forms (4.8). It is easy to show that these functions satisfy:

$$(D^2-\lambda^2)X+MY=0, \tag{A 1}$$

$$(D^2-\lambda^2)^2 Y-M^{-1}R\lambda^2 X=0, \tag{A 2}$$

$$X=Y=DY=0 \quad (z=0), \tag{A 3}$$

$$DX+LX=Y=D^2Y+\lambda^2X=0 \quad (z=1). \tag{A 4}$$

Here $D=d/dz$, $\lambda=s_{mi}/a$, and the Rayleigh number R is considered to be the eigenvalue. The adjoint problem follows from (5.7)–(5.11), (5.13), and satisfies

$$(D^2-\lambda^2)X^*+M^{-1}R\lambda^2Y^*=0, \tag{A 5}$$

$$(D^2-\lambda^2)^2 Y^*-MX^*=0, \tag{A 6}$$

$$X^*=Y^*=DY^*=0 \quad (z=0), \tag{A 7}$$

$$DX^*+LX^*+\lambda^2DY^*=Y^*=D^2Y^*=0 \quad (z=1). \tag{A 8}$$

Solutions for X, Y, X^*, Y^* were determined using the Fourier-series method of Nield (1964).

We use the normalizations

$$X=1 \quad (z=1), \tag{A 9}$$

$$X^*=1 \quad (z=1). \tag{A 10}$$

REFERENCES

Bénard, H. 1900 *Rev. Gen. Sci. Pure Appl.* **11**, 1261.

Davis, S. H. 1969 *J. Fluid Mech.* **39**, 347.

Davis, S. H. & Homsy, G. M. 1980 *J. Fluid Mech.* **98**, 527.

Eckhaus, W. 1965 *Studies in Non-Linear Stability Theory*. Springer.

Koschmieder, E. L. 1967 *J. Fluid Mech.* **30**, 9.

Kraska, J. R. & Sani, R. L. 1979 *Int. J. Heat Mass Transfer* **22**, 535.

Liang, S. F., Vidal, A. & Acrivos, A. 1969 *J. Fluid Mech.* **36**, 239.

Nield, D. A. 1964 *J. Fluid Mech.* **19**, 341.

Palmer, H. & Berg, J. 1971 *J. Fluid Mech.* **47**, 779.

Pearson, J. R. A. 1958 *J. Fluid Mech.* **4**, 489.

Rosenblat, S. 1979 *Stud. Appl. Math.* **60**, 241.

Rosenblat, S., Homsy, G. M. & Davis, S. H. 1981 *Phys. Fluids* **24**, 2115.

Scanlon, J. W. & Segel, L. A. 1967 *J. Fluid Mech.* **30**, 149.

Scriven, L. E. & Sternling, C. V. 1964 *J. Fluid Mech.* **19**, 321.

Smith, K. A. 1966 *J. Fluid Mech.* **24**, 401.

Sørensen, T. S. (ed.) 1979 *Dynamics and Instability of Fluid Interfaces*, Lecture Notes in Physics, vol. 105. Springer.

Vidal, A. & Acrivos, A. 1966 *Phys. Fluids* **9**, 615.

Zeren, R. & Reynolds, W. C. 1972 *J. Fluid Mech.* **53**, 305.